UNIVERSIDADE D
COIMBRA

Pedro Diogo Jesus Lourenço

# TOOL ASSISTED FRICTION WELDING OF MILD STEEL

**Dissertação no âmbito do Mestrado Integrado em Engenharia Mecânica, no ramo de Produção e Projeto orientada pela Professora Doutora Dulce Maria Esteves Rodrigues e pelo Doutor Sree S. Sabari e apresentada ao Departamento de Engenharia Mecânica da Faculdade de Ciências e Tecnologia da Universidade de Coimbra**

Julho de 2021

FACULDADE DE CIÊNCIAS E TECNOLOGIA
UNIVERSIDADE D COIMBRA

# TOOL ASSISTED FRICTION WELDING OF MILD STEEL

Submitted in Partial Fulfilment of the Requirements for the Degree of Master in Mechanical Engineering in the speciality of Production and Project

## Tool Assisted Friction Welding de Aço Macio


**Author**

**Pedro Diogo Jesus Lourenço**

**Advisors**

**Professora Doutora Dulce Maria Esteves Rodrigues**

**Doutor Sree Sabari Shunmugam**


**Jury**

| | |
|---|---|
| **President** | **Professora Doutora Cristina Maria Gonçalves dos Santos**<br>**Professora Auxiliar da Universidade de Coimbra** |
| **Vowel** | **Professor Doutor Carlos Miguel Almeida Leitão**<br>**Professor Adjunto do Instituto Superior de Engenharia de Lisboa** |
| **Advisor** | **Professora Doutora Dulce Maria Esteves Rodrigues**<br>**Professora Associada com Agregação da Universidade de Coimbra** |

**Coimbra, Jully, 2021**

# ACKNOWLEDGEMENTS

The realisation of this work would not have been possible without the support and collaboration of some people, whom I could not forget to thank:

First of all, to my family, in special to my parents, Fernando and Helena, for all the help, support and knowledge. I cannot thank you enough. I hope they are proud of their son achievement. I would like to extend my thanks also to my brother, Tiago.

To Professor Dulce Rodrigues and Professor Sree Sabari the supervisors of this thesis, for all the knowledge shared, encouragement and patient, without which it would be impossible to achieve this feat.

To all my high school and university friends, especially to Carlos, Gabriel, Rute, João, Mariana, Joana, Alexandre, Tiago, Pedro and Diogo for all the adventures, support, friendship, and good moments during the past years who changed me. Thank you to my second family.

To David, Professor Ivan and Professor Carlos, for all the answered questions and continuous help during this investigation, for the good work environment and funny moments made this dissertation's development even more special. About the good work environment, I need thanks also to Engineer Rui and to Neves Manuel.

A final thanks go to Ana for being my support, care, patience and love, a very special thank you.

# Abstract

The present work aimed to analyse the thermomechanical conditions in Tool Assisted Friction Welding (TAFW) of mild steel, by relating the process parameters with output parameters, namely, the torque and the temperature. With this objective, linear lap welds were made in 1 mm thick plates of DC01 carbon steel. The process parameters considered in the investigation were the rotational and the traverse speeds and the tool diameter. The temperature evolution during welding was registered using a thermographic camera and the torque evolution was acquired from the welding equipment. Transverse cross-sections of the welds were cut for morphological analysis and the strength of the joints was assessed by performing tensile-shear tests. The strain distribution in the samples, acquired using Digital Image Correlation (DIC), was used in order to determine the local properties of the weld. Finally, an analysis of the torque and of the temperature evolutions, with process parameters, was also made to understand the influence of the process parameters on the joints properties.

The results obtained allowed to conclude that lap welding of 1 mm thick steel plates may be carried out successfully by TAFW, using a penetration depth of only 0.1 mm. It was also found that both the traverse and rotational speeds have an important influence on the temperature distribution during welding, and in this way, on the morphology of the process affected zone (PAZ). For a constant traverse speed, the increase in the rotational speed conducts to an increase of the welding temperature. On the other hand, for a constant tool rotational speed, the increase of the traverse speed conducts to a decrease of the welding temperature. Independently of the rotational speed, all the welds produced with 1400 mm/min traverse speed were defective or not welded. All the other welds produced with the 16 mm diameter tool have strength similar to that of the base material. It was also found that the tool diameter, axial force and rotational speed strongly influence the welding torque.

**Keywords** Torque, Temperature, TAFW, Steel, Lap Welding.

# Resumo

O presente trabalho teve como objetivo analisar as condições termomecânicas durante a soldagem por Tool Assisted Friction Welding (TAFW), relacionar os parâmetros de entrada com os principais parâmetros de saída: binário e temperatura. Com este objetivo, foram realizadas soldaduras lineares em juntas sobrepostas utilizando um aço-carbono, DC01, com espessura de 1 mm, como material base. Os parâmetros dos processos considerados na investigação foram a velocidade de rotação e de avanço e o diâmetro da ferramenta. A evolução da temperatura durante a soldadura foi registada por uma câmara termográfica e a evolução do binário por o equipamento de soldadura. As secções transversais das soldaduras foram cortadas para fazer uma análise metalográfica, e uma análise da resistência da soldadura caracterizada pela realização de ensaios transversais de tração-cisalhamento. Durante os ensaios foi usada a aquisição de dados de deformação por Digital Image Correlation (DIC). A análise de sensibilidade do binário e da temperatura foi feita, de forma a perceber a influência dos parâmetros de entrada nas propriedades das soldaduras.

Os resultados obtidos permitiram concluir que a soldadura sobreposta por TAFW em placas de aço com 1 mm de espessura e uma penetração inferior a 0.1mm podem ser realizadas com sucesso. Verificou-se também que as velocidades quer de avanço quer de rotação têm importante influência na distribuição da temperatura durante o processo, que está relacionada com a morfologia da zona afetada pelo processo (PAZ). Para uma velocidade de avanço constante o aumento da velocidade de rotação promove o aumento da temperatura do processo. Por outro lado, para uma velocidade de rotação da ferramenta constante, o aumento da velocidade de avanço promove uma diminuição de temperatura Independentemente da velocidade de rotação, todas as soldaduras produzidas a uma velocidade de 1400 mm/min apresentam defeitos ou não estão soldadas. No entanto todas as outras soldaduras produzidas com a ferramenta de 16 mm de diâmetro apresentam uma curva de Força-Deformação semelhante á do material base. Verificou-se também que a força axial, o diâmetro da ferramenta e velocidade de rotação têm forte influência na evolução do torque.

**Palavras-chave:** Binário, Temperatura, Aço, TAFW, Junta sobreposta.

# Contents

# LIST OF FIGURES

# LIST OF TABLES

# LIST OF SIMBOLS AND ACRONYMS/ ABBREVIATIONS

## List of Symbols

v - Traverse Speed [mm/min]

$a$ - Tool tilt angle [º]

ω - Rotational Speed [rpm]

$F_z$ - Axial Force [N]

$d_z$ - Plunge Depth [mm]

pi - Plunge In [s]

wt - Welding Time [s]

po - Plunge Out [s]

dt - Dwell Time [s]

## Acronyms/Abbreviations

FSW - Friction Stir Welding

SSW - Solid-State Welding

AS - Advancing Side

RS - Retreating Side

FSSW- Friction Stir Spot Welding

FSP- Friction Stir Processing

TAFW - Tool Assisted Friction Welding

PCBN- Polycrystalline Cubic Boron Nitride

PAZ- Process Affected Zone

UTS- Ultimate Tensile Strength

DIC - Digital Image Correlation

NYL- Normalised Yield Load

NML- Normalised Maximum Load

# 1. INTRODUCTION

Wayne Thomas developed the Friction Stir Welding (FSW) process, at The Welding Institute (TWI), in 1991. This process is considered a suitable alternative to fusion welding, especially, for the joining of aluminium alloys. This process, which also presents higher energy efficiency than the fusion welding processes, makes use of a non-consumable tool, animated by translational and rotational movements, to promote the joining of the base materials by stirring under intense plastic deformation.

The Tool Assisted Friction Welding (TAFW) technology, recently developed at the University of Coimbra, by Mira-Aguiar et al., 2016, is very similar to the FSW process, differing from it by the fact that it uses tools without pin and with a flat shoulder. For this reason, the main joining mechanism responsible for the welding in TAFW is the atomic diffusion taking place at the high temperature and pressure exerted by the tool. No base materials stirring, or inter-mixing occurs during TAFW, as in FSW, which enables to suppress important lap joint defects, such as the hooking. Another FSW defect that does not happen in TAFW is the keyhole left by the pin at the end of the weld, as in FSW.

In the present work, lap welds were produced, using the TAFW technology, in 1 mm thick plates of DC01 mild steel, in order to analyse the influence of process parameters, namely, the traverse and the rotational speeds and the tool diameter, on the quality of the joints. The work plan also envisaged to assess the evolution of the thermal and mechanical conditions during the welding process. The thermal cycles were acquired using a thermographic camera and the output torque was obtained from the welding machine. The process-induced transformations, on the base metal, were evaluated by performing metallographic analysis. Mechanical characterisation of the joints, using the tensile-shear tests, was also performed.

The dissertation is divided in 5 chapters. After an initial introduction, in chapter 1, the state of the art is presented in chapter 2. The chapter starts by describing the FSW and TAFW technologies and discussing the main differences and similarities between them. The operating principles of the two technologies are described, as well as some works alluding to the application of these welding processes. Chapter 3 describes the experimental

procedure, along with the equipment used in the investigation, the process parameters and the base material. The discussion of the results is developed in chapter 4, where the results of the morphological and microstructural analysis of the welds, and the mechanical characterisation, are displayed, as well as the temperature and the torque data. Finally, in chapter 5, the main conclusions of the present investigation and some recommendations for future work, inside the same field of investigation, are presented.

,

# 2. STATE OF THE ART

## 2.1. The Welding Process

Friction Stir Welding (FSW) is a Solid-State Welding (SSW) process developed by Wayne Thomas, at The Welding Institute, in 1991 (Patent Number - US5460317A). SSW joining processes are carried out at temperatures below the melting temperature, which enables avoiding several defects related to the melting of the base materials, and in this way, offering better joint quality. Furthermore, using SSW processes, it is possible to join different grades of non-ferrous alloys, which is very complex to be done by fusion welding (Vural, 2014). In addition to other SSW processes capabilities, FSW has superior energy efficiency, and it allows the joining of a larger range of joint configurations. FSW does not require the addition of filler materials, fluxes or shielding gases [(Bhushan & Sharma, 2019) (Mishra & Ma, 2005)].

According to Thomas et al., 2003, FSW is a process that uses a non-consumable cylindrical tool, made of a material harder than the workpiece material to be welded, for producing the joint. During the welding, the tool has rotational and traverse speed movements, which allow the heating of the workpiece by friction and plastic deformation, as well as the stirring of the base materials to be joined along linear paths. It is a process which is becoming widely used in the industry, mainly for the joining of aluminium alloys. The ease of being automated, also makes the FSW process very interesting.

As shown in Figure 2-1, the FSW tool usually consists of a cylindrical shoulder with a concentric cylindrical pin. There are different geometries for both the shoulder and the pin. The absence of pin is a possibility as well. However, according to Elangovan et al., 2008 and Rai et al., 2011, any changes in the tool geometry may influence the heat generation, the traverse force, the torque, the flow of the base material, as well as the thermomechanical environment as a whole.

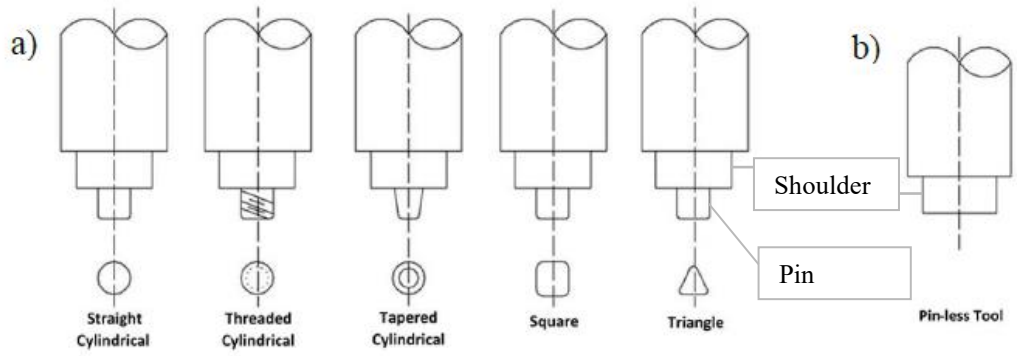


**Figure 2-1:** (a)Examples of different types of pin tools. (b) Pin-less tool. (Adapted from Elangovan et al., 2008)

The Rotational Speed (ω) of the tool in contact with the plate is the responsible for the heating of the base material by friction, and consequently, by its softening, allowing its stirring by the tool. The stirring action takes place all across the base material thickness due to the presence of the pin. In addition, the traverse speed (v) of the tool allows performing linear welding. These two speeds, the rotational and the traverse, are essential welding parameters, as they have a strong influence on the thermal cycles, i.e., on the heat generation and dissipation during welding. Other parameters to consider are the axial force ($F_z$), the tool tilt angle (α) and the plunge depth of the tool in the material base ($d_z$). Figure 2-2 shows a scheme of the process, in which the different FSW parameters are identified. The Advancing Side (AS) and the Retreating Side (RS) of the weld are also identified in the figure. The AS is the side of the weld where the rotational and the linear velocity of the tool have the same direction and the RS is the side where the opposite occurs.

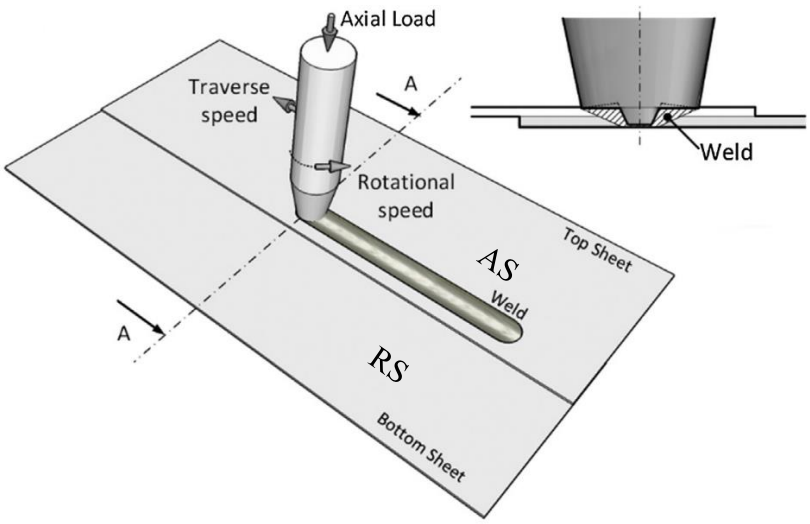


**Figure 2-2:** Scheme of the FSW process, and the parameters. **(**Adapted from Mira-Aguiar et al., 2016)

Figure 2-3 shows the cross-sections and the surface of welds produced by FSW. Images a) and b) correspond to welds without defects. The other images display welds with different types of defects. According to El-Sayed et al., 2021, the typical FSW defects are tunnel, flash, kissing bond, void, groove, hooking and lack of penetration.

FSW process features several variants, like the Friction Stir Spot Welding (FSSW) and the Friction Stir Processing (FSP) technologies. FSSW is a process with the same operating principles of the FSW process but made by points. In this case, the tool has only the vertical linear movement, required for the positioning of the tool, and the rotational movement, required to heat the base material by friction and for mixing it by plastic deformation. The tool penetration and the dwell time, i.e., the period of time that tool remains in contact with the base material, are crucial parameters (Nguyen et al., 2011 and Lakshminarayanan et al., 2015). Mishra & Ma, 2005 introduced the FSP technique. FSP is not aimed at welding, but rather at improving the surface or bulk properties of the processed materials. Once again, a rotating tool is inserted into the material to be processed, generating heat and intense plastic deformation and, therefore, promoting recrystallisation.

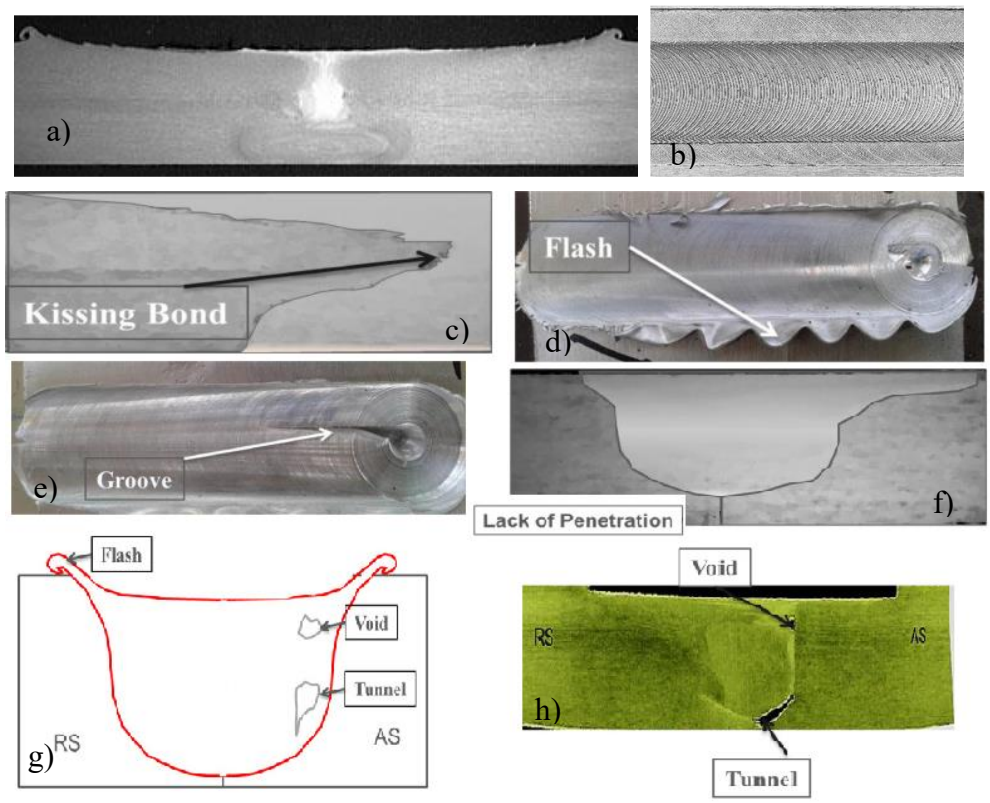


**Figure 2-3:** The cross-section and surface of the weld produced by FSW (a and b), and some typical defects FSW (c to h). (Adapted from El-Sayed et al., 2021; and Thomas et al., 2003).

Tool Assisted Friction Welding (TAFW) is another variant of the FSW process, proposed by Mira-Aguiar et al., 2016, for the linear lap welding of very thin plates. As FSSW and FSP, the TAFW process also has the same operating principles of FSW. However, the tool used in TAFW has a particularity, it does not have a pin and the shoulder has a flat surface, with no features. The absence of the pin and the flat geometry of the shoulder lead to joining mechanism different from that promoted by the FSW tools. While in FSW, the joining results from the stirring of the base materials across the abutting interface, in TAFW, the joining is caused by the pressure and the temperature, following mechanisms similar to that operating in Friction Welding (FW). Andrade et al., 2018 also proved that during TAFW there is no stirring or inter-mixing of the base materials, as happens in FSW.

The use of TAFW, despite being limited to the lap joining of thin plates, has some advantages compared to FSW. Namely, the use of pinless tools has the advantage of preventing tool pin damage/wear, which, according to Rai et al., 2011, is one of the most critical limitations for the welding steels by FSW. The suppression of the pin is also desirable to simplify the production of the tools. In steel welding, for example, those tools are usually made in tungsten, tungsten alloys and PCBN, which makes it difficult to manufacture and very expensive. Finally, since no base materials stirring occurs during TAFW, this technique allows to overcome some typical friction stir lap welding defects, such as the hooking, at one or both sides of the weld, and the keyhole left by the tool at the end of the weld (Mira-Aguiar et al., 2016).

In Forcellese et al., 2012, the effect of pin and pinless tool geometries and size, on the properties of friction stir welds in AZ31 magnesium alloy thin sheets was investigated. The authors concluded that a more homogeneous microstructure is obtained when using the pinless tool. Furthermore, they also discovered that increasing the diameter of the pinless tools promote a beneficial effect on the ductility and strength of the joints. Bakavos et al., 2011 also used pinless tools, with flat, scrolled and fluted features, for the spot welding of thin aluminium plates. According to the authors, the welds produced with the pinless tools, with a flat surface, were free from defects. However, introducing fluted features machined on the tool surface, changes the base material flow, enabling the use of faster welding velocities.

In Andrade et al., 2021, linear lap welds in thin plates of galvanised steel were produced using TAFW. No hooking or cold lap defects were observed for any of the lap

welds, and it was concluded that the zinc had an important influence on the contact conditions at the tool-workpiece interface, affecting the thermo-mechanical conditions developed during welding.

According to several authors (Andrade et al., 2018; Kim et al., 2017; Mira-Aguiar et al., 2016), the microstructural evolution in the through-thickness direction, observed from the centre of the TAFW joints, is characterised by structures with decreasing grain size, from top to bottom.

## 2.2. Torque and Temperature

The proper application of FSW requires identifying the primary process parameters (input parameters) controlling the heat generation and dissipation during the process, as well as the amount of material stirred by the tool. As already explained, there are three basic process parameters used for the control of the FSW process: the rotational and the traverse speeds, as well as the plunge depth, when welding in position control, or the axial force, when welding in force control.

Oakes & Landers, 2009 developed and implemented a general tracking controller for regulating the axial force. The authors concluded that, as the plunge depth is increased, the axial force increases and eventually reaches a steady value. Ni et al., 2020 studied the influence of the welding parameters on the axial force, in micro pinless friction stir welding of a 0.5 mm thick 7075-T6 aluminium alloy plates. According to the authors, the axial force increases, when the welding speed is increased, and decreases, when the rotational speed is increased. They also concluded that the axial force affects the heat generation, and in this way, the welds quality. When the axial force is not enough, the heat production and the pressure may be insufficient, which easily causes voids and kissing bond defects. On the other hand, when the axial force is too high, defects such as flash are prone to occur.

Several authors analysed the viability of using the tool torque as a process output parameter able to be used as an indicator of the thermomechanical conditions developed during FSW. For example, Longhurst et al., 2010 proposed the use of the torque, instead of the axial force, as a process control parameter. The results obtained by the authors show that the torque is more sensitive to the variation of the tool depth than the axial force. Another

conclusion is that the torque control also provides a method to regulate the weld power, since the weld power is predominately a function of the torque and of the tool rotational speed. Leitão et al., 2012, in FSW of non-heat-treatable (AA5083-H111) and heat-treatable (AA6082-T6) aluminium alloys, depicted a strong sensitivity of the torque to the welding conditions. According to these authors, when welding defects are formed, strong variations in the torque are registered. The authors also identified a strong influence of the rotational speed and of the thickness of the base materials on the torque. According to them, the torque becomes smaller when decreasing the plates thickness or increasing the rotational speed. This conclusion was also reported by Galvão et al., 2012, in a study on the torque sensitivity to the welding conditions in dissimilar FSW of aluminium and copper. Leitão et al., 2012 and Galvão et al., 2012 also concluded that the transverse speed has no significant influence on the torque. In order to analyse the influence of the process parameters on the FSW torque and temperature, a literature review was performed by Andrade et al., 2020. The authors found that meanwhile the tool rotational speed has an important influence on the heat generation, the tool dimensions have a significant influence on both the heat generation and on the volume of material being stirred during welding.

It is also well known that the temperatures reached during the welding process influence the microstructure and the mechanical properties of the welds. In order to evaluate the frictional heat generation in FSW of steels, a pinless tool was used by Andrade et al., 2019. According to the authors, the main factors influencing the frictional heat generation are the tool diameter, the tool rotational speed and the presence of low melting point coatings at the tool-workpiece interface. The authors registered a threshold in the maximum temperature, for each tool diameter, which increases with increasing tool diameters. They also concluded that the maximum welding temperature varied according to the base material and the tool rotational speed, for the smaller tool diameters.

Bachmann et al., 2017 developed a temperature control system, based on an analytical torque model, and observed that the welds produced with this control system displayed higher quality, and higher homogeneity, than welds performed using conventional control procedures. Silva-Magalhães et al., 2019 developed a temperature-control strategy, for the robotic FSW in industrially relevant conditions. Their study demonstrated the ability to join highly complex geometries by using temperature feedback control. As a result, both time and cost reduction were achieved. In addition, the FSW temperature controller was able

to maintain consistent weld quality along the entire joint length, with the exception of areas affected by equipment limitations.

# 3. EXPERIMENTAL PROCEDURE

In this work, lap welds were produced, by TAFW, in 1 mm thick mild steel sheets (DC01), which chemical composition is described in Table 1.

**Table 1:** Chemical composition of the base material, DC01 [%]

| Material | C | Mn | P | S | Si | Cr | Al |
|---|---|---|---|---|---|---|---|
| DC01 | 0.050 | 0.210 | 0.016 | 0.008 | 0.010 | 0.030 | 0.048 |

All welding trials were performed using a *MTS I-STIR PDS* dedicated FSW machine. The plates were cleaned before performing the welds in order to remove rust, oil and corrosion particles, avoiding any chemical or mechanical interferences in the welding process. All welds were produced in position control.

## 3.1. Process Parameters

In the present work, the tool was tilted backwards by 2º. Two different pinless tools with flat shoulder were used, which were named as PL12 and PL16. The name of each tool indicates the geometry and the diameter of the shoulder surface. “PL” indicates that the shoulder geometry is flat without features or grooves, and “12” is the value of the diameter in millimetres. Both tools were made in Tungsten Carbide, known for performing well at elevated temperatures, due to its high wear resistance and reasonable fracture toughness. The welding parameters tested are that presented in Figure 3-1. Namely, the influence of the tool diameter, on the welding conditions, was tested using tool rotational (ω) and traverse (v) speeds of 1000 rpm and 600 to 1400 mm/min, respectively. The analysis of the influence of traverse speed and rotational speed on the welding conditions was performed using the PL16 tool and raging the speeds from 600 to 1400 mm/min and from 800 to 1600 rpm.

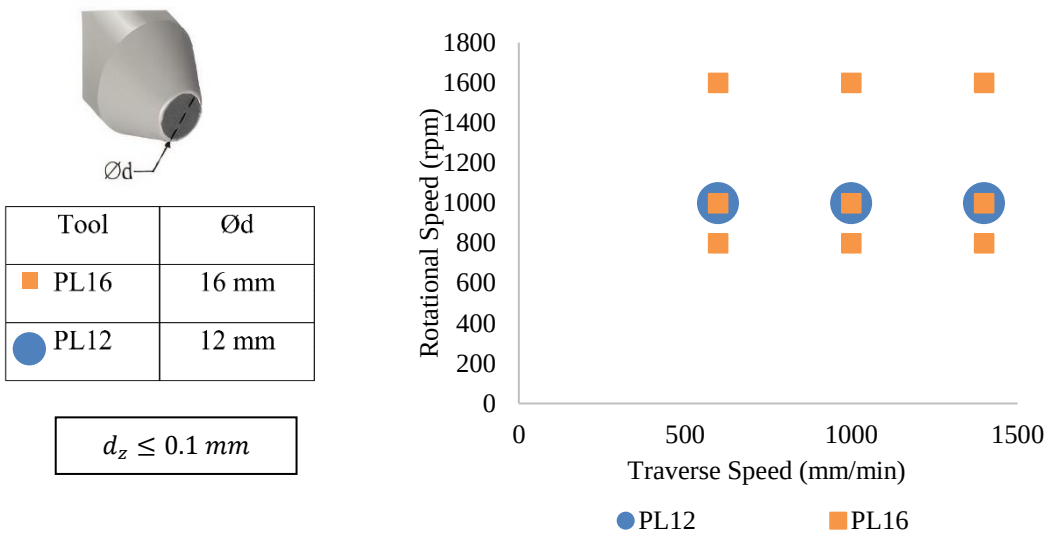


**Figure 3-1:** Process parameters (Tool Diameter, Rotational and Traverse Speeds).

## 3.2. Post-Processing Procedures

The torque and the force evolutions were obtained from the welding machine. Furthermore, in real-time, the temperature evolution was registered with a thermographic camera, "FLIR A655sc", positioned 0.5 m away from the tool, in order to reduce the effect of the reflections on the acquisition. Finally, the information was organised in "Microsoft Excel" Worksheets, used to perform the post-processing of the temperature and of the torque data, i.e., for plotting the temperature and torque evolution, with the tool displacement, and calculating the maximum and the average values for each welding condition.

### 3.2.1. Torque Data

The TAFW process can be divided into four stages, the Plunge In(pi), the Dwell Time (dt), the Welding Time (wt) and the Plunge Out (po). Figure 3-2 illustrates the four different stages. The Plunge In is the stage during which the tool moves vertically, penetrating the upper plate, until the defined plunge depth value is reached. The Dwell Time is the stage during which the tool, animated exclusively with rotational speed, is in contact with the base material. The welding time is the stage during which the tool remains in contact with the top plate, animated with the traverse and rotational speeds required for promoting the joining.

The Plunge out stage corresponds to the end of the welding, when the tool is removed from the base material.

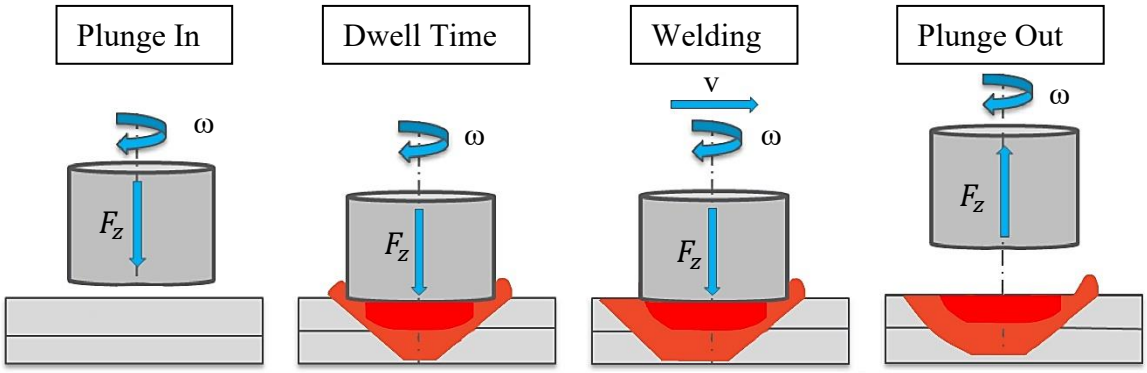


**Figure 3-2:** Scheme of different phases during the TAFW. (Adapted from El-Sayed et al., 2021)

The torque output signal was recorded, in all TAFW tests, with a frequency of 20Hz. The torque evolution graphics, in Figure 3-3, are an example of the standard evolution of the torque with the tool displacement (Figure 3-3-a) and the time (Figure 3-3-b). The analysis of Figure 3-3-b enables to identify three of the four TAFW stages described above.

For each set of welding conditions tested in the current work, the torque-time and torque-distance analysis was made, allowing to obtain the maximum and average values of the torque to be used in the sensitivity analysis.

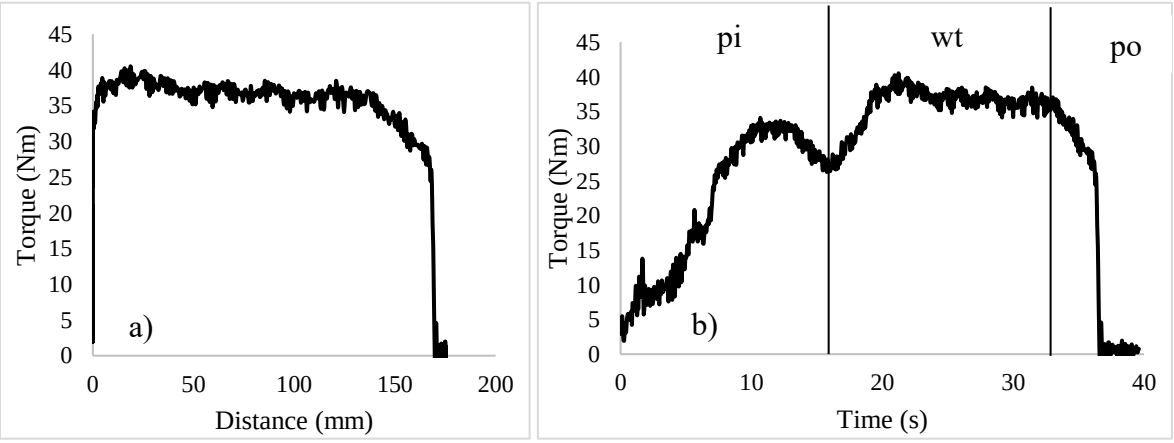


**Figure 3-3:** Torque curve, example during TAFW. Torque-Distance and Torque-Time. Legend: pi= Plunge In, wt= Weld Time, po=Plunge Out.

### 3.2.2. Temperature Data

The thermal cycles, i.e., the evolution of the temperature with the time, determine the final microstructure and the strength of the welds. In Figure 3-4 are shown examples of the evolution of the temperature with the tool displacement (Figure 3-4-a) and with the time (Figure 3-4-b). Meanwhile, the first graphic enables to conclude that there were no important differences in temperature, between the start and the end of the weld, the thermal cycle enables to identify three of the four TAFW stages described previously.

For each set of welding conditions, the temperature-time and the temperature-distance analysis was made, allowing to obtain the maximum and the average values of the temperature to be used in the sensitivity analysis.

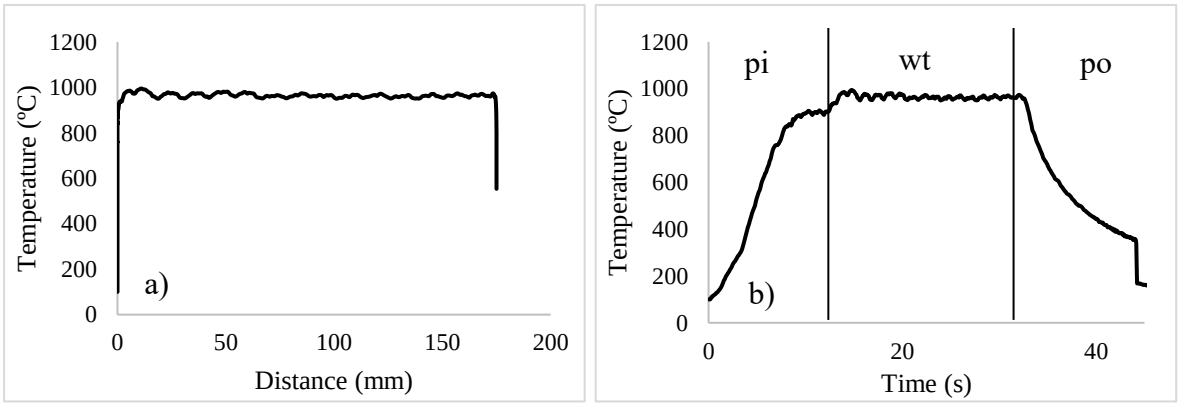


**Figure 3-4:** Temperature curve, example during TAFW. Temperature-Distance and Temperature-Time. Legend: pi= Plunge In, wt= Weld Time, po=Plunge Out.

### 3.2.3. Morphological Analysis

After the welds were made, some measurements were taken. First, the width of the welds was measured and then, it was compared for the different welding conditions. Measurements were taken in the weld crown, in three different locations, at the central part of the weld length, and averaged for each weld.

After the dimensional control, seven samples, each 12 mm wide (as Figure 3-5 shows), were cut from each of the welds. The samples were used in the microstructural examination and in the mechanical testing tasks. Three samples were used to perform AS tensile-shear tests and the other three for RS tests.

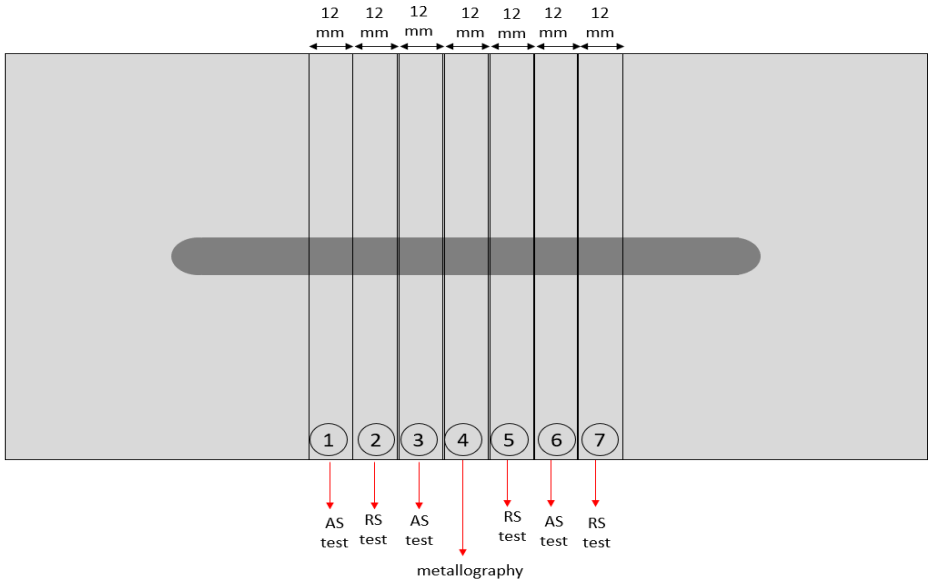


**Figure 3-5:** Scheme of extraction of sample for the microstructural examination and shear testing.

### 3.2.4. Metallographic and Microstructural Analysis

For each weld, a sample was used to perform the metallographic analysis, allowing to visualise the microstructure and characterising the transformations induced by the process on the base material. For this analysis, an optical microscope was used, "Leica 4000 M LED". The transverse microstructure of the welds was revealed after polishing and applying a chemical, Nital 2% (98ml ethanol + 2 ml HNO3). The Nital solution is responsible for the etching of the steel, revealing the microstructure. The application of the chemical in the sample was made by immersing the sample into the Nital solution for 20 seconds.

### 3.2.5. Mechanical Characterisation

The strength of the overlapped joints was evaluated by performing tensile-shear tests in a universal tensile machine, "SHIMADZU AUTOGRAPH AGS-X 100 kN". The use of the optical strain gauge "GOM ARAMIS 5M" allowed the acquisition of strain distribution maps on the front surface of the specimens, using digital image correlation (DIC). According to the procedures described in Costa et al., 2015, due to the strength asymmetry between the AS and RS sides of the lap welds, two different types of tensile–shear samples should be tested, as schematised in Figure 3-6. At least two samples of each type were tested. All the tests were performed in quasi-static loading conditions (5 mm/min), at room temperature.

Strain data analysis was performed following the procedures detailed in Leitão et al., 2012. Before testing, the specimens were prepared by applying a random black speckle pattern, over the previously mat white painted surface, in order to enable strain data acquisition by DIC.

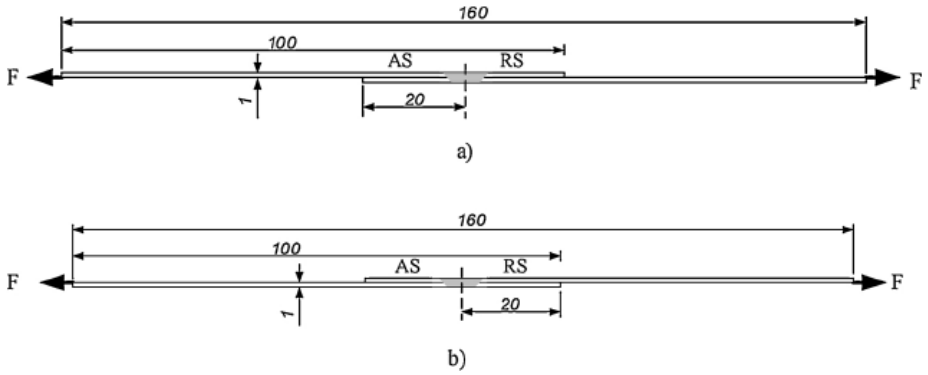


**Figure 3-6:** Scheme of the advancing (a) and retreating (b) lap shear samples. [Andrade et al., 2018]

# 4. ANALYSIS OF RESULTS

In order to enable a better understanding of the experimental results, this chapter will be divided into three subchapters. In the first subchapter, the results of the Morphological and Microstructural Characterisation of the welds are shown, enabling a comparative analysis of the process affected zone of the different welds. In the second subchapter, the mechanical characterisation results are displayed and discussed. In the third subchapter, the torque and temperature evolutions with process parameters are discussed and the results are related with the welds properties.

## 4.1. Morphological and Microstructural Characterisation

In order to illustrate the influence of the tool diameter on the welds properties, transverse cross-sections of the welds produced with the PL12 and PL16 tools, at a rotational speed of 1000 rpm and traverse speeds of 600, 1000 and 1400 mm/min, are compared in Figure 4-1. The figure shows, for each weld, a large Process Affected Zone (PAZ), with microstructure contrasting with that of the base material. As in Mira-Aguiar et al., 2016, a continuous dark line, aligned with the abutting plate's initial interface, is also visible in all the images. According to the authors, the dark line consists of remnants of the base metals surface oxides. The higher magnification of the joint interface, represented in Figure 4-2, for the weld produced with the PL16 tool at 800 rpm and 600 mm/min, shows that despite the presence of the oxide layer, there is microstructural continuity across the interface. No voids were observed inside the dark line for any of the welds.

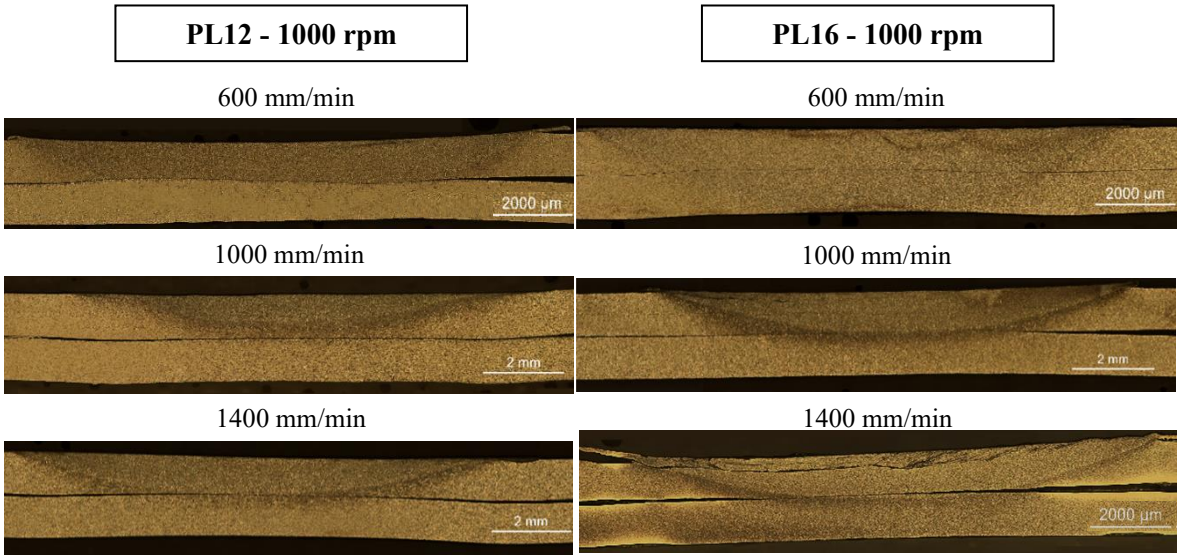


**Figure 4-1:** Cross-sections of the welds manufactured with two different tools (PL12 and PL16), at a rotational speed of 100 rpm and traverse speeds of 600, 1000 and 1400 mm/min.

According to Mira-Aguiar et al., 2016, the presence of the continuous dark line in all the cross-sections indicates that no vertical material flow took place from the upper to the lower plate, or vice-versa, proving that the weld does not result from the base materials stirring, as in FSW. In addition, no hooking defect can be observed in any of the cross-sections in Figure 4-1, which is another indicator of the absence of material flow across the faying interface. Analysing carefully the figure it is also possible to depict differences in the PAZ morphology between the welds produced with the different tools or the different traverse speeds. From the analysis of the cross-sections, it is also possible to conclude that the thickness reduction in the weld zone, relative to the base material plates, was almost zero for all the welds. A significant reduction of the height of the PAZ was registered when the traverse speed was increased from 600 to 1000 mm/min, but no significant difference in the height of the PAZ was registered when increasing the traverse speed from 1000 to 1400 mm/min.

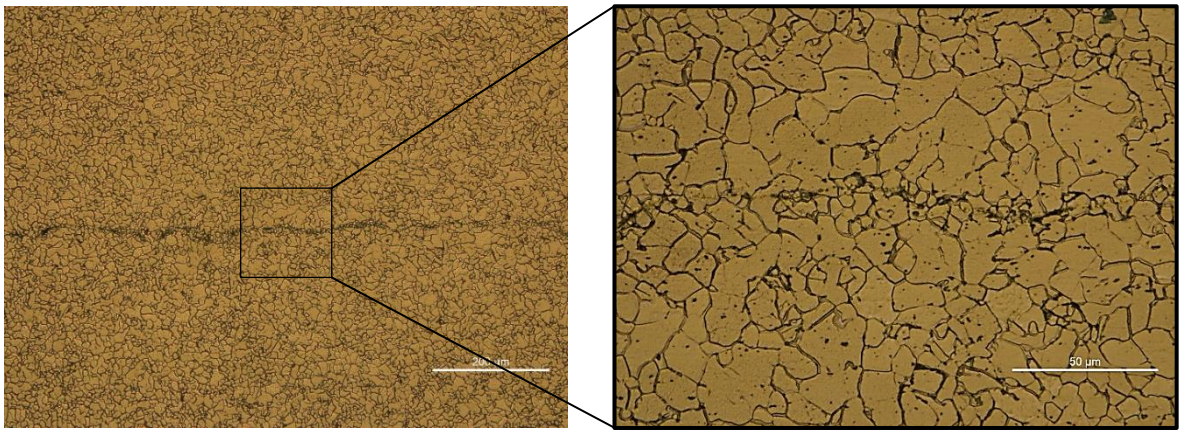


**Figure 4-2:** Bonding interface for the weld produced with the PL16 tool at 600 rpm and 800 mm/min.

Figure 4-3 shows graphics with the evolution of the height and width of the PAZ as a function of the traverse speed and the tool diameter. It is possible to conclude that the PAZ of the welds produced with the tool with the larger diameter (PL16) are not much deeper or wider than the ones produced with the smaller diameter tool (PL12), as observed in Figure 4-1.

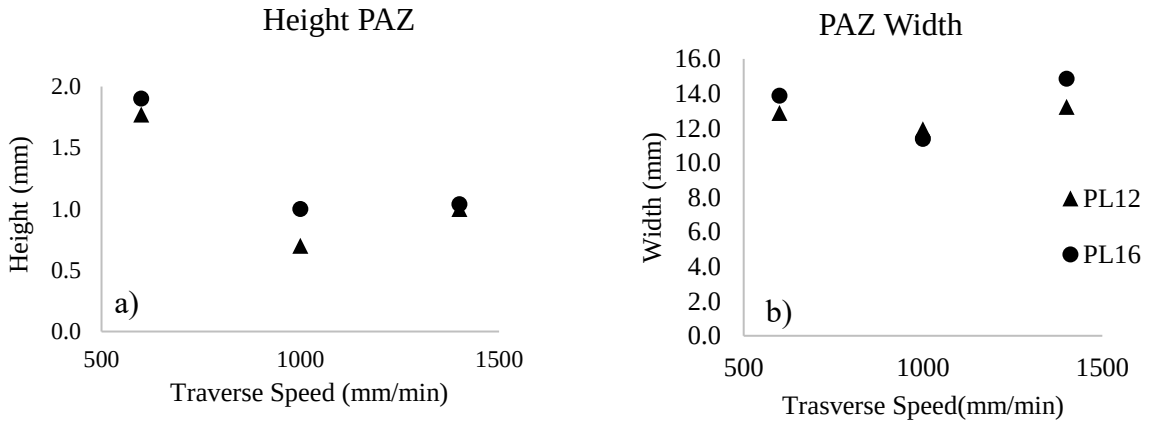


**Figure 4-3:** Graphics a) PAZ Depth-Traverse Speed; b) PAZ Width-Traverse Speed

The influence of the rotational speed on the PAZ morphology may be depicted by analysing Figure 4-4 to 4-6. Each figure consists of macrographs of the transverse cross-sections of the welds produced with the PL16 tool, with the same traverse speed, but different rotational speeds (800, 1000 and 1600 rpm). The traverse speed used to produce the welds in Figure 4-4 was 600 mm/min, in Figure 4-5 was 1000 mm/min and in Figure 4-6 was 1400 mm/min. The figures also show the measurements of PAZ height (h). The first conclusion

which can be taken from the analysis of the figures is that the reduction in thickness in the weld, relative to the base material, is almost zero. Figure 4-6 also shows that the welds manufactured with 1400 mm/min had hooking, flash defects, voids or are not joined.

Figure 4-4 to 4-6 also show that, independent of the traverse speed, the width of the PAZ was wider for the welds produced with the lower rotational speeds (800 rpm and 1000 rpm). When the traverse speed was increased from 600 mm/min (Figure 4-4) to 1000 mm/min (Figure 4-5), the width and the height of the PAZ decreased, but when the traverse speed was increased from 1000 (Figure 4-5) to 1400 mm/min (Figure 4-6), no important differences in the PAZ dimensions were registered.

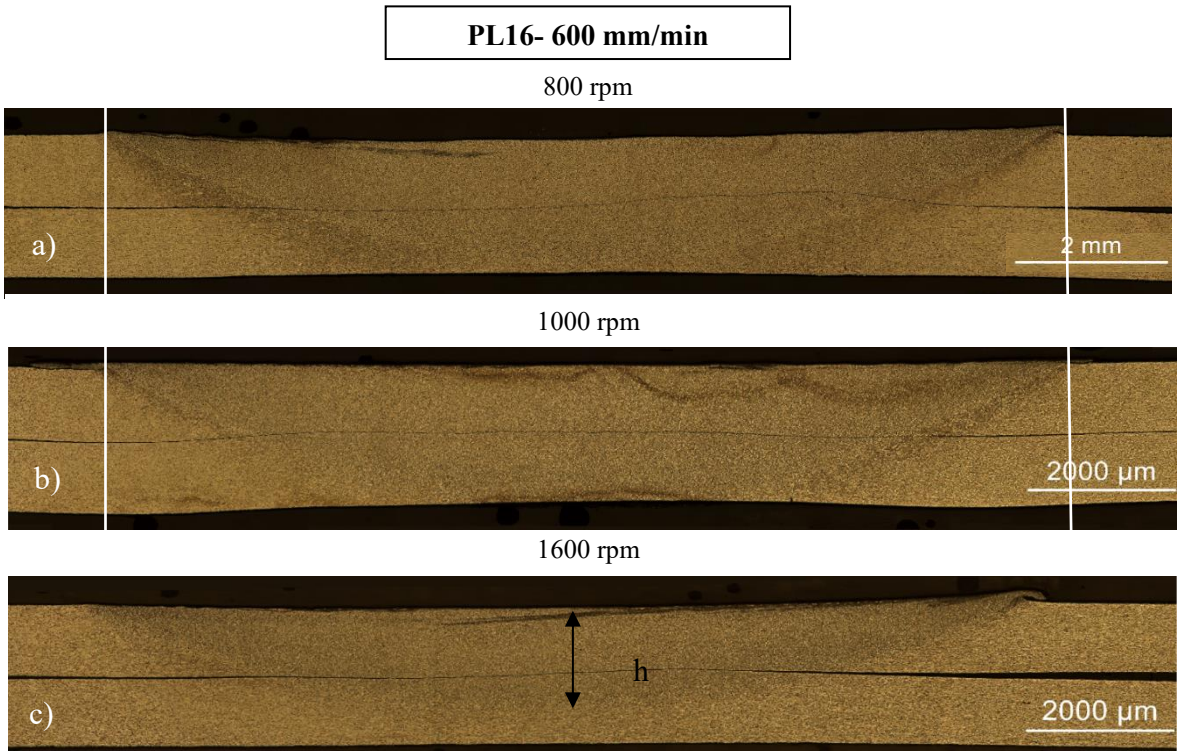


**Figure 4-4:** Cross-sections of the welds manufactured with PL16 tool, 600 mm/min and varying the rotational speed.

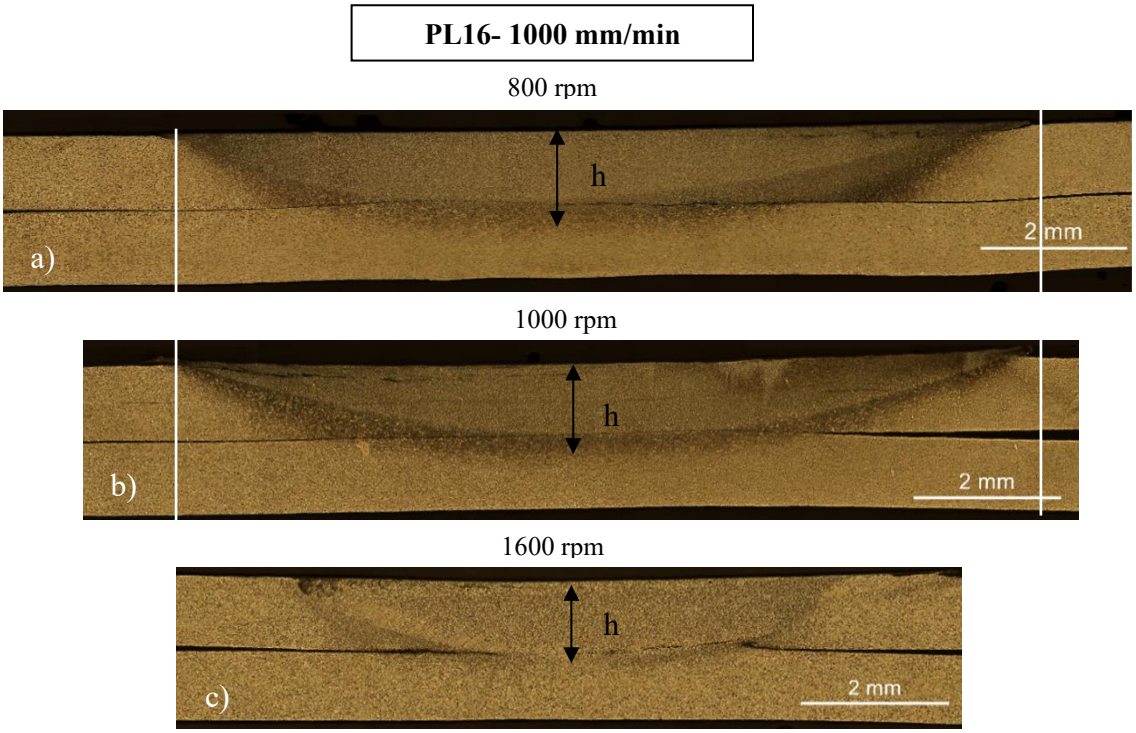


**Figure 4-5** Cross-sections of the welds manufactured with PL16 tool, 1000 mm/min and varying the rotational speed.

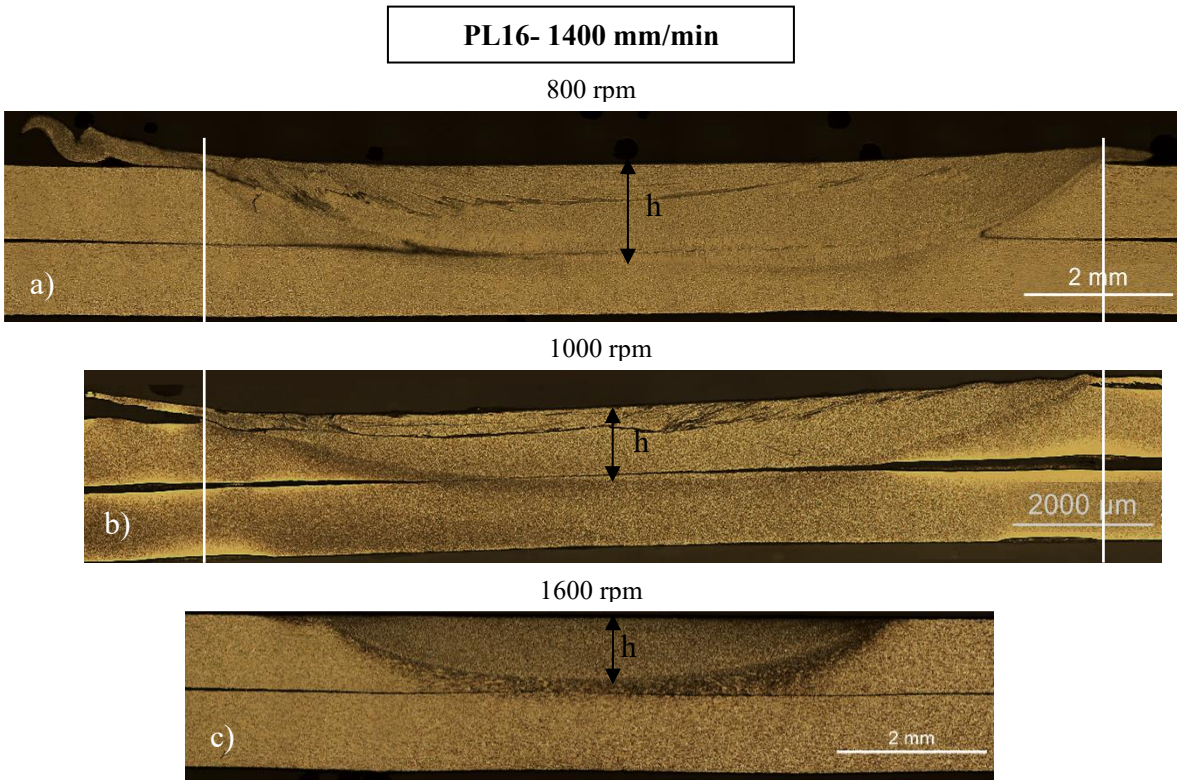


**Figure 4-6:** Cross-sections of the welds manufactured with PL16 tool, 1400 mm/min and varying the rotational speed.

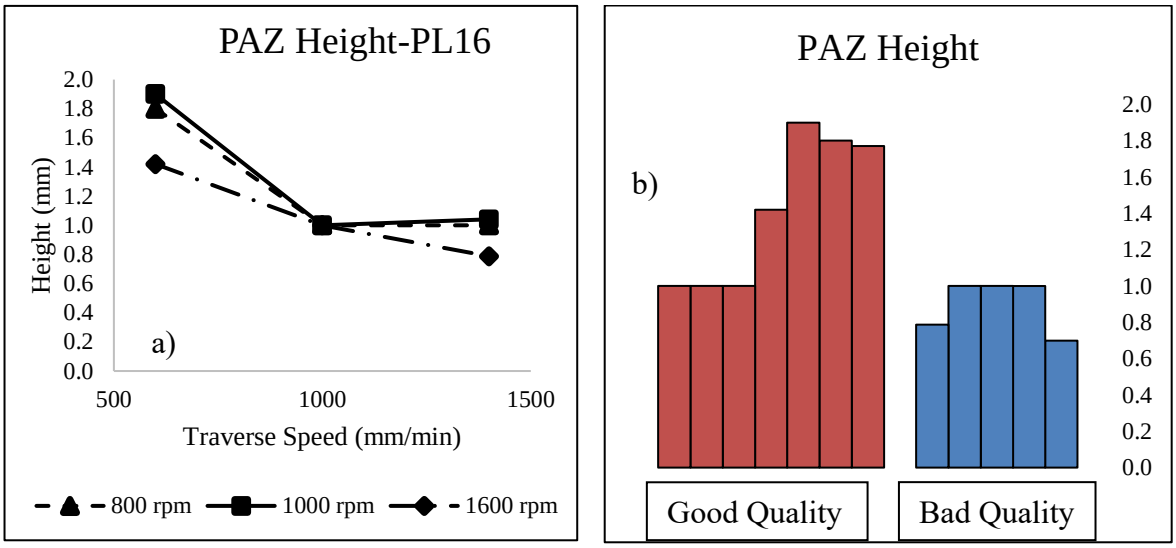


**Figure 4-7:** Graph evolution of PAZ with the different rotational speed and traverse speed using PL16 (a). Evolution of PAZ Height with de quality of the weld (b).

The evolution of the PAZ height as a function of the rotational and traverse speeds is shown in Figure 4-7-a). This figure shows that the height of the PAZ decreases when the traverse speed increases from 600 (Figure 4-4) to 1000 mm/min (Figure 4-5), but did not change when the traverse speed was further increased to 1400 mm/min (Figure 4-6). Another interesting conclusion is that when the traverse speed is 1000 mm/min (Figure 4-5), all the values of PAZ height are practically equal to 1 mm, with no influence of the rotational speed variation.

The height of the PAZ is essential to guarantee the good quality of the joints. If the height of the PAZ does not exceed the thickness of the upper plate, reaching the second plate, no sound joining between the plates may occur. This is demonstrated in Figure 4-7-b, which shows that all the welds with bad quality are produced with a PAZ height equal or inferior to 1mm. The joints were classified as having bad quality since the plates were separated during the handling of the samples to metallographic analysis, before this specific analysis. The welds produced with the traverse speed of 1000 mm/min, the PAZ, despite having a lower height than the welds made at 600 mm/min, still reach the second plate. When the traverse speed was 1400 mm/min, the PAZ height is similar compared with the PAZ height of the welds made in 1000 mm/min, but when the rotational speed is 1000 rpm, the

plates are not joined, and when the rotational speed was 1600 rpm the PAZ did not reach the second plate.

Figure 4-8 to Figure 4-10 show details of the microstructure of the base material and of the welds made with a rotational speed of 800 rpm and traverse speeds of 600 mm/min and 1000 mm/min, respectively. These welds were selected for a deeper analysis, due to the important differences in the PAZ microstructure between them and the good quality of the joints depicted in the visual inspection. It is also important to enhance that the same features of the PAZ displayed in Figure 4-9 were observed for all the welds manufactured at 600 mm/min. The same is valid for the welds manufactured at 1000 mm/min.

In the magnifications a) and b), in Figures 4.9 and 4.10, which correspond to the microstructure of the AS and RS of the welds, it is possible to observe the limits of the region with a refined microstructure. Actually, comparing the microstructures in Figure 4-9 and Figure 4-10, with the base material microstructure in Figure 4-8, it can be concluded that the grain size of the base material is larger than that of the PAZ. The magnifications c), d) and e) show the microstructure evolution in the middle of the weld across the PAZ thickness. Both figures show an evident microstructural gradient across the thickness, characterised by structures with decreasing grain size from the top to the bottom of the PAZ, as in Mira-Aguiar et al., 2016. Comparing the top PAZ grain size, in Figure 4 9 and Figure 4 10, it can also be concluded that the grain size for the weld produced with the slower traverse speed is larger. No difference is observed when comparing the AS (a) and the RS (b) sides, in each figure (4-9, 4-10), proving that the heat generation/distribution was symmetrical between the AS and RS sides of the tool.

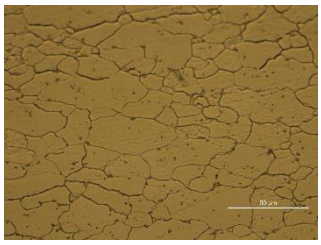

**Figure 4-8:** Details of the microstructure of the base material, far from PAZ.

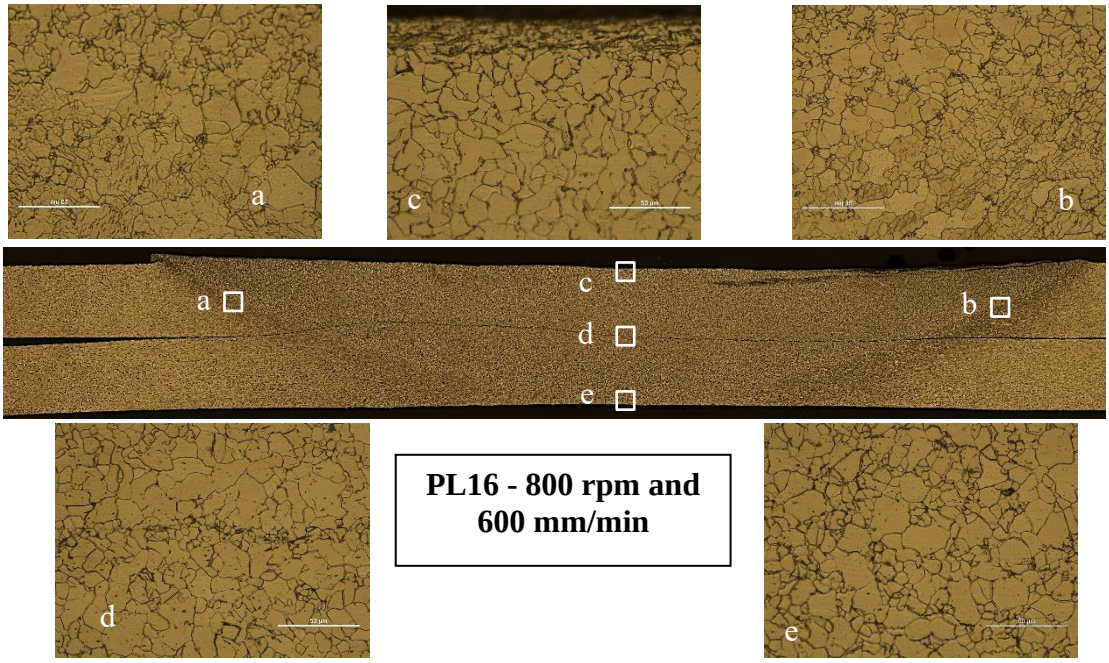


**Figure 4-9:** Details of the microstructure of the weld PL16 - 800 rpm and 600 mm/min.

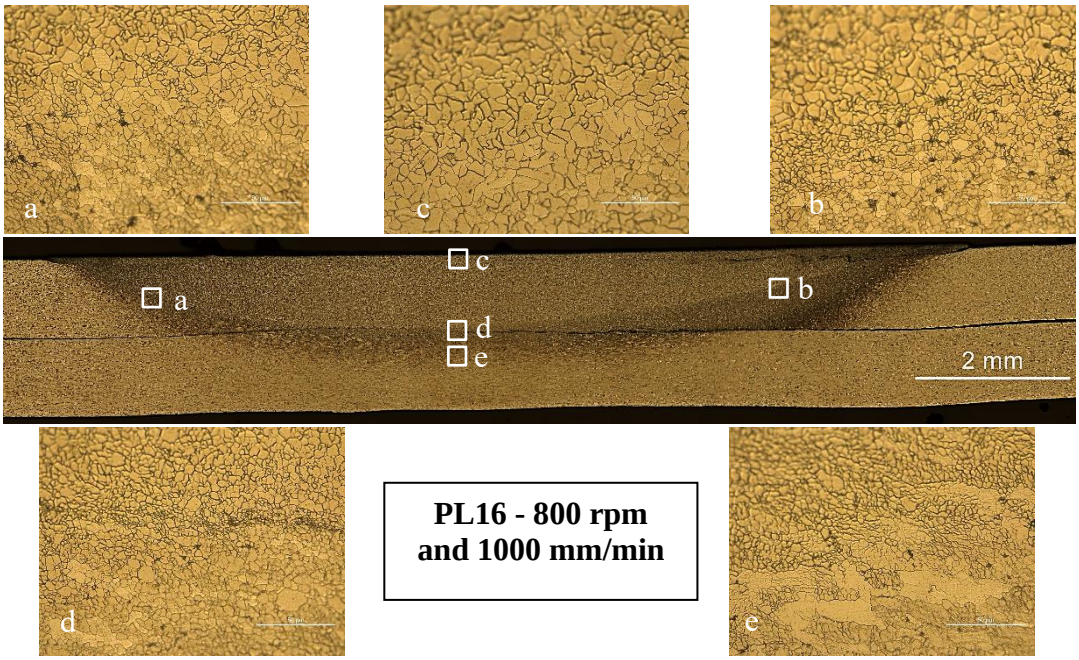


**Figure 4-10:** Details of the microstructure of the weld PL16 - 800 rpm and 1000 mm/min.

The analysis of the figures also enables to conclude that meanwhile, in Figure 4-9, the PAZ encompasses the entire thickness of both plates, in Figure 4-10, the PAZ ends up at the top of the second plate. However, the magnification of the interface in Figure 4-10-d) shows that, despite of this, the plates were joined.

Figure 4-11 shows details of the microstructure of the weld made with a PL16 tool at a rotational speed of 1000 rpm and traverse speed of 1400 mm/min. The magnifications a) and b), which correspond to the microstructures at the RS and AS of the welds, show the limits of the region with a refined microstructure. The magnifications c), d) and e) show the microstructure evolution in the middle of the weld across the PAZ thickness showing an evident microstructural gradient across the thickness, characterised by structures with decreasing grain size from the top (c) to the bottom of the PAZ (d). Unfortunately, this weld had several defects: voids (f), flash defects (1mm length) and some stirred material (c, a). The magnification d) shows that the plates were not joined.

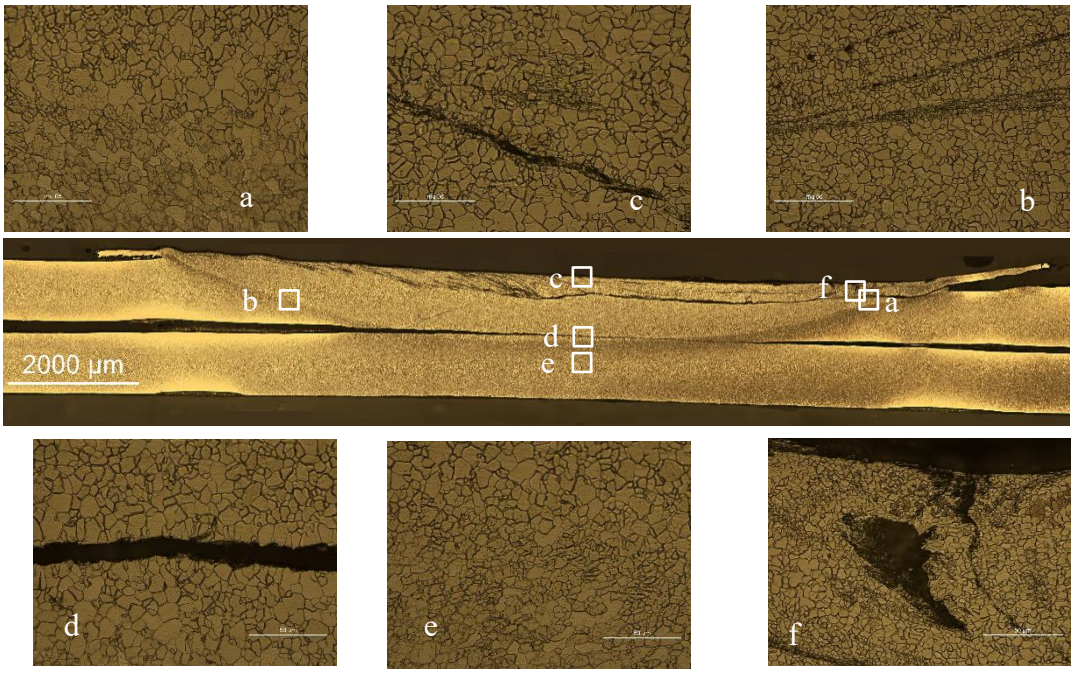


**Figure 4-11:** Details of the microstructure of the weld PL16 - 1000 rpm and 1400 mm/min.

## 4.2. Mechanical Characterisation

As described in the experimental procedure, the strength of the dissimilar joints was assessed by performing tensile–shear tests of AS and RS samples. The welds which were identified in Figure 4-7, as having bad quality, were not tested in tension since they failed during the handling of the samples for metallographic analysis.

Figure 4-12 to Figure 4-14 show the load-displacement curves registered in the tensile-shear tests of the welds produced with the PL16 tool at 600 mm/min and 1600 rpm

(Figure 4-12), 1000 mm/min and 1000 rpm (Figure 4-13) and 1400 mm/min and 1000 rpm (Figure 4-14). In each graphic it is also plotted the force-displacement curve corresponding to a homogeneous base material specimen, with the same width of the lap shear samples. Analysing the load-displacement curves in Figure 4-12 and Figure 4-14 it is possible to conclude that they have shape and values similar to the load-displacement curve of the base material, with no relevant differences between the AS and the RS. In Figure 4-12-a), the displacement is higher in the AS and in Figure 4-13-a) the displacement is higher in the RS, showing no direct relationship between displacement and the tested side. The Mises strain distribution map, at the maximum load, shown in images (b) of Figure 4-12 and 4-13, and the photographs of the fractured samples, shown in the image (c) of each figure, show that these welds failed in the base material for very low values of plastic deformation in the weld.

Analysing now the load-displacement curves in Figure 4-14, it is possible to conclude that this weld failed, for much low displacement values than the ones in Figures 4-12 and 4-13, by separation of the plates along the lap interface (Figure 4-14-c), which indicates that the bonding was restricted to a very small length. In spite of this, none of the samples had failed before some plastic deformation took place in the base material.

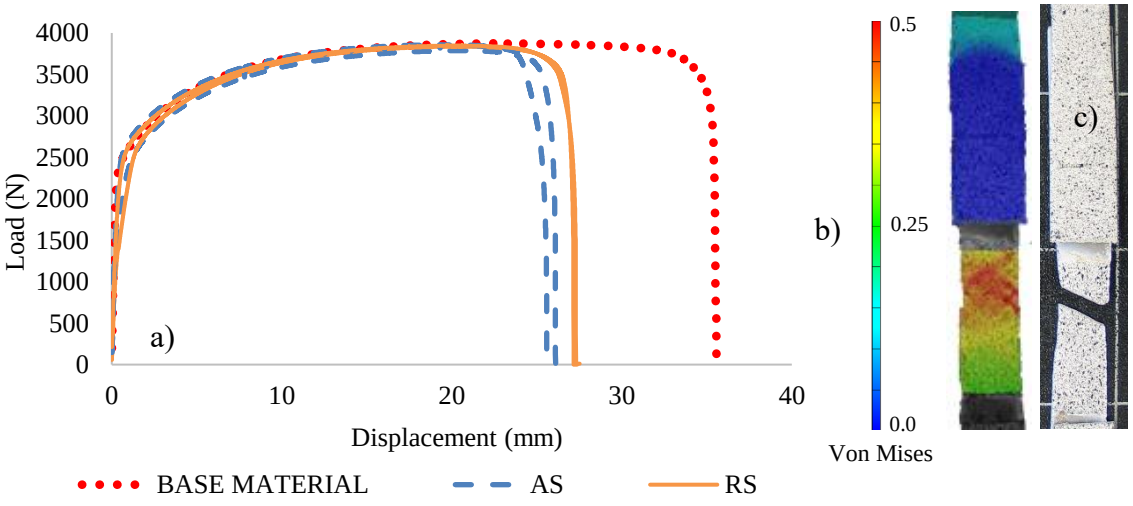


**Figure 4-12:** Load-Displacement curve (a), DIC strain distribution map (b) and fractured sample (c) for the weld produced with the PL16 tool at 600 mm/min and 1600 rpm.

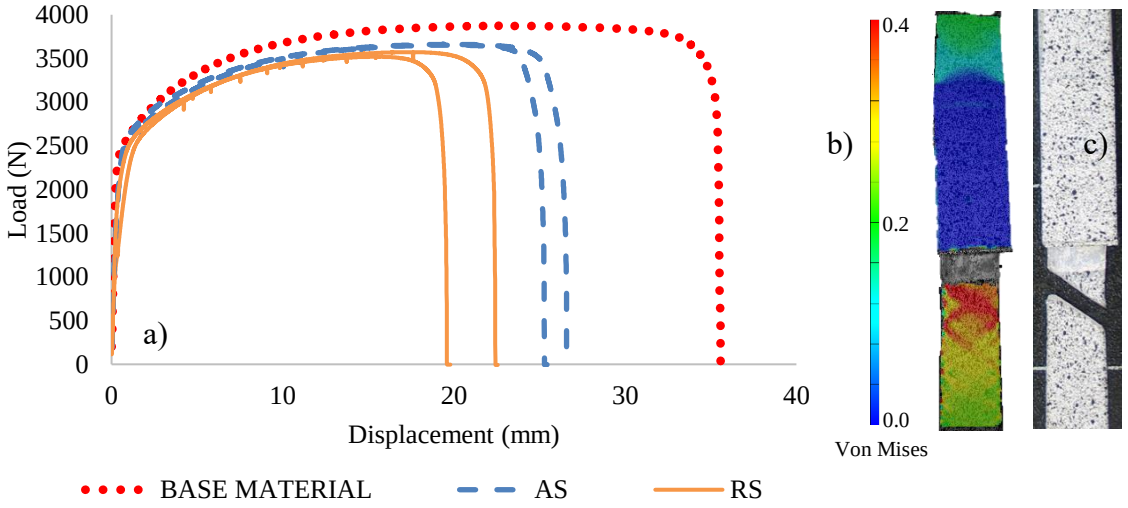


**Figure 4-13:** Load-Displacement curve (a), DIC strain distribution map (b) and fractured sample (c) for the weld produced with the PL16 at 1000 mm/min and 1000 rpm.

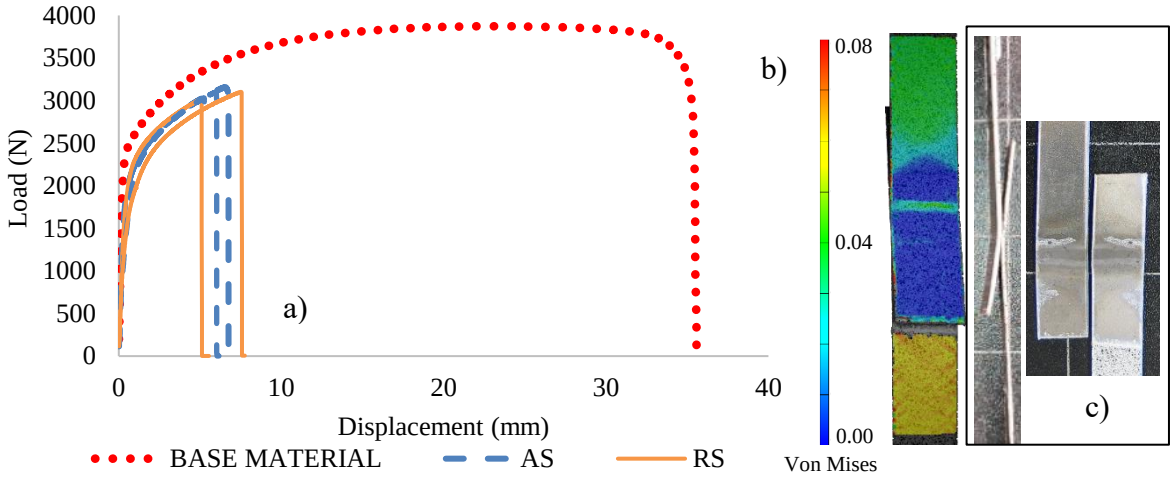


**Figure 4-14** Load-Displacement curve (a), DIC strain distribution map (b) and fractured sample (c) for the weld produced with the PL16 at 1400 mm/min and 1000 rpm.

The analysis of all the mechanical testing results enabled to conclude that all samples, except the weld produced with the PL16 tool at 1400 mm/min and 1000 rpm, which failed by separation of the plates at the bonding interface, had lap shear strength similar to the ultimate tensile strength (UTS) of the base material. The failure modes were also similar for the AS and RS samples. No important differences in the lap shear strength of the AS and RS samples were reported, as is usual in lap welds produced by FSW.

As in Costa, et al., 2015, two parameters were calculated in order to characterise the welds strength, the Normalised Yield Load (NYL) and the Normalised Maximum Load (NML) parameters, determined according to the equations:

$$NYL = \frac{F_{Yield}^{Weld}}{F_{Yield}^{BM}}; \quad (1)$$

$$NML = \frac{F_{máx}^{Weld}}{F_{máx}^{BM}}; \quad (2)$$

In the previous equations, the $F_{Yield}^{Weld}$ and $F_{Yield}^{BM}$ correspond to the yield load registered in the tensile-shear test of the weld and in the tensile test of the Base Material (DC01), respectively. The $F_{máx}^{Weld}$ and $F_{máx}^{BM}$ correspond to the maximum load registered in the tensile-shear test of the weld and in the tensile test of the Base Material, respectively.

All the results obtained in the tensile-shear tests are shown in Table 2, together with the AS and RS normalised loads for each weld. The normalised load values are also plotted in Figure 4-15, as a function of the speed ratio (ω/v). Analysing this figure, it is possible to conclude that the welds produced with the slower traverse speed had the higher NYL and NML values. The maximum values of NYL and NML were registered for the welds produced with the maximum "ω/v", i.e, when the weld pitch increases, the normalised loads also increase. This result is directly related to the traverse speed, since when the weld pitch is higher, the traverse speed (different colours in the graphic) is lower. The welds produced at 1400 mm/min had lower strength, especially for the NYL, showing a maximum yield strength of 72% compared with the base material yield strength. The rotational speeds did not seem to have a clear influence on the welds produced at 600 mm/min. The increase of the rotational speed decreased the normalised loads on the welds produced at 1000 mm/min.

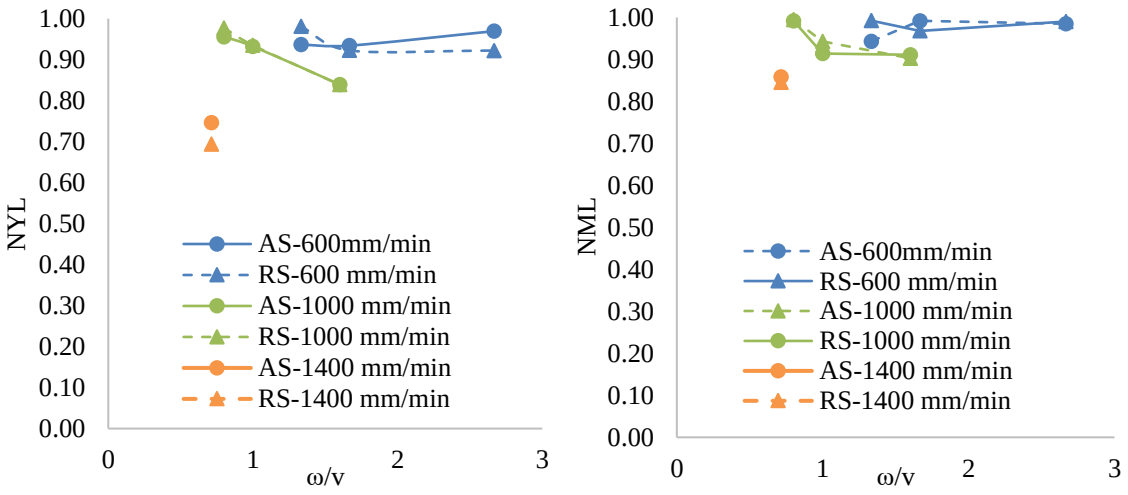

**Figure 4-15:** NML and NYL versus the weld pitch (w/v). Advancing (AS) and Retreating (RS) sides

**Table 2:** Results obtained in the tensile-shear tests: Maximum and Yield Load, Normalized Values Load.

| Tool | Traverse Speed [mm/min] | Rotational Speed [rpm] | AS / RS | Maximum Load [N] | Yield Load [N] | NML | NYL |
|---|---|---|---|---|---|---|---|
| BASE MATERIAL | | | | 3880 | 2842 | | |
| PL16 | 600 | 800 | AS | 3451 | 2520 | 0.94 | 0.91 |
| | | | | 3866 | 2654 | | |
| | | | RS | 3843 | 2727 | 0.99 | 0.95 |
| | | | | 3857 | 2691 | | |
| | | 1000 | AS | 3850 | 2636 | 0.99 | 0.91 |
| | | | | 3847 | 2524 | | |
| | | | RS | 3757 | 2592 | 0.97 | 0.9 |
| | | | | 3753 | 2503 | | |
| | | 1600 | AS | 3786 | 2655 | 0.98 | 0.94 |
| | | | | 3857 | 2700 | | |
| | | | RS | 3835 | 2590 | 0.99 | 0.9 |
| | | | | 3857 | 2700 | | |
| | 1000 | 800 | AS | 3854 | 2577 | 0.99 | 0.93 |
| | | | | 3866 | 2702 | | |
| | | | RS | 3850 | 2702 | 0.99 | 0.95 |
| | | | | 3846 | 22697 | | |
| | | 1000 | AS | 3653 | 2531 | 0.94 | 0.91 |
| | | | | 3661 | 2619 | | |
| | | | RS | 3572 | 2590 | 0.91 | 0.91 |
| | | | | 3519 | 2574 | | |
| | | 1600 | AS | 3505 | 2307 | 0.9 | 0.82 |
| | | | | 3499 | 2329 | | |
| | | | RS | 3528 | 2268 | 0.91 | 0.82 |

| | | | | | | | |
|---|---|---|---|---|---|---|---|
| | | | | 3541 | 2365 | | |
| | 1400 | 1000 | AS | 3160 | 2131 | 0.86 | 0.72 |
| | | | | 3160 | 1989 | | |
| | | | RS | 3016 | 2131 | 0.84 | 0.67 |
| | | | | 3541 | 1703 | | |

The welds analysed displayed an excellent strength, being obtained an average value of 95% compared with the base material strength. The NML value is higher than the NYL for all the welds, demonstrating that welds had plastic deformation before failure.

Excluding the weld produced at 1400 mm/min, all welds strength is over 90% of the base material ultimate strength. Once again, excluding the weld produced at 1400 mm/min and the weld produced at 1000 mm/min and 1000 rpm, the yield strength of other welds is over 90% when comparing with the base material, obtaining an average value of 88% considering all the welds.

## 4.3. Torque and Temperature Analysis

An analysis of torque and temperature evolution with the welding conditions in Tool Assisted Friction Welding (TAFW) is made in this subchapter. More precisely, understanding the influence of the traverse and rotational speeds, and the tool diameter, on these two output parameters, and relating it with the analysis made before, concerning the morphological and mechanical characterisation, is the objective of this subchapter.

The graphic in Figure 4-16 shows the evolution of the output parameters axial force, temperature and torque, with the tool displacement. In the graphic it is also plotted the evolution of the traverse with the tool displacement. The curve enables to conclude that the tool attained the prescribed speed of 1000 mm/min after some displacement took place and started decreasing the traverse speed before the end of the weld. Attending to this, in the graphic, it is signalised, with a blue rectangle, the portion of the weld effectively produced with the traverse speed of 1000 mm/min. In order to ensure that all the results displayed in the dissertation were relative to the traverse speed prescribed in the experimental plan, the same type of graphic in Figure 4-16 was plotted for all the welding conditions tested in the dissertation. Using those graphics, the values of the average torque and of the average

temperature, which will be analysed in the next, were calculated as the average of the torque and temperature values registered when the traverse speed is equal to the prescribed value. The obtained average torque and temperature values are shown in Table 3.

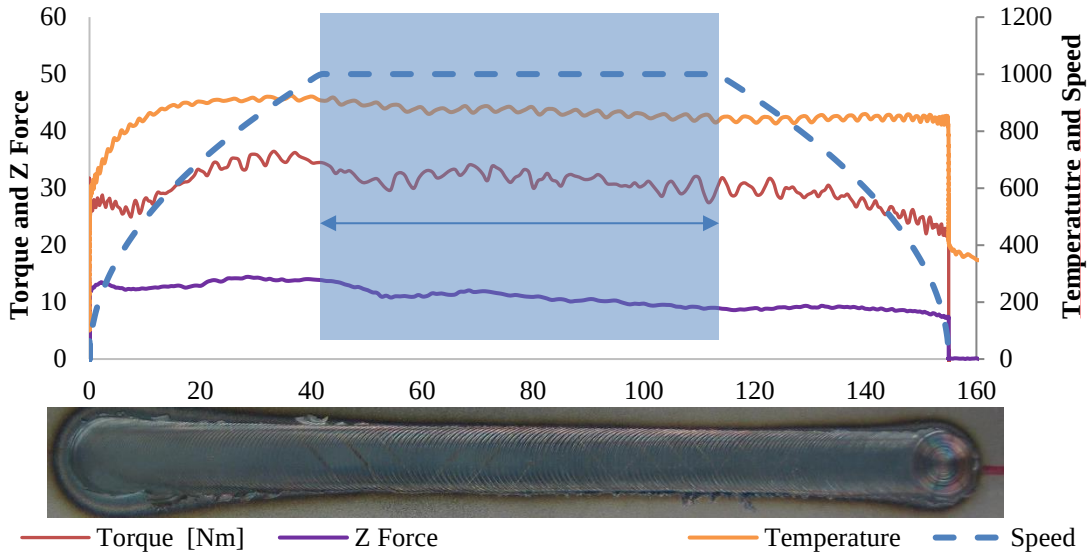


**Figure 4-16:** Evolution of Torque (Nm), Z Force (N), Temperature (ºC) and Traverse Speed (mm/min).

**Table 3:** Average Torque and Temperature on the different parameters used to produce the welds.

| Tool | Traverse Speed (mm/min) | Rotational Speed (rpm) | Average Torque (N) | Average Temperature (ºC) |
|---|---|---|---|---|
| PL16 | 600 | 800 | 37.1 | 964 |
| | | 1000 | 30.9 | 985 |
| | | 1600 | 20.3 | 1023 |
| | 1000 | 800 | 31.6 | 818 |
| | | 1000 | 31.6 | 872 |
| | | 1600 | 14.9 | 844 |
| | 1400 | 800 | 46.7 | 805 |
| | | 1000 | 35.5 | 867 |
| | | 1600 | 14.8 | 764 |

### 4.3.1. Torque Evolution with Process Parameters

The evolution of the average torque with the ratio (ω/v) is shown in Figure 4-17-a) and the evolution of the average torque with the tool diameter, at the same traverse speed, is shown in the graphic of Figure 4-17-b). Analysing Figure 4-17-a), it is possible to conclude that a decrease in the average torque occurs when the rotational speed increases. On the other hand, the traverse speed does not have such an evident influence on the torque.

Analysing Figure 4-17-b), relative to the evolution of the average torque with tool diameter, it is possible to conclude that the tool diameter influences the torque values. For all the welds made at different traverse speeds, the average torque is bigger when the diameter of the tool used is larger.

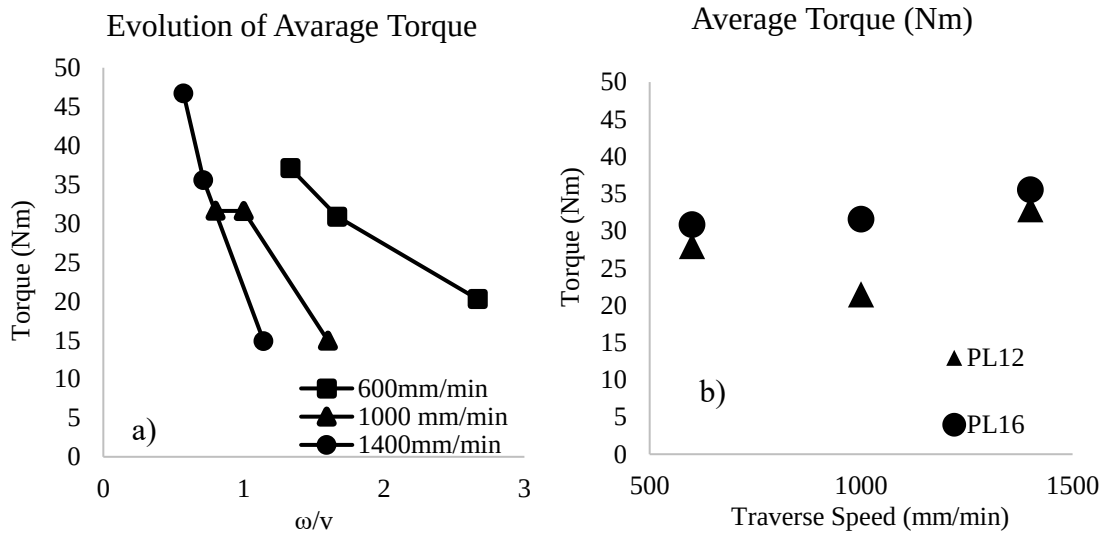


**Figure 4-17:** Evolution of Torque with the speed ratio (ω/v) (a) and with the tool diameter (b) at the same traverse speed.

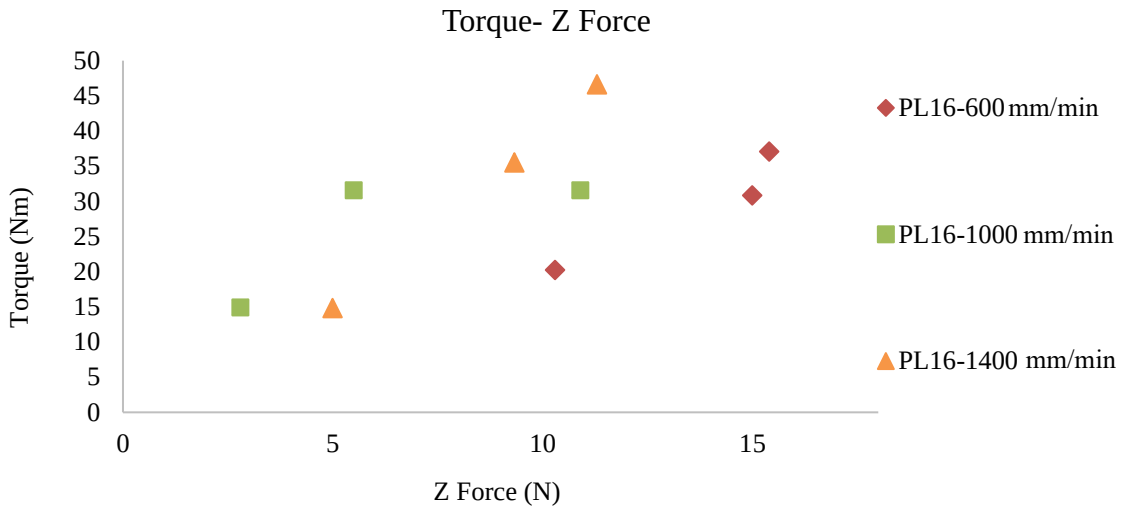


**Figure 4-18:** Evolution of Torque with the Z Force.

Figure 4-18 shows the average torque values versus the average axial force for all the welding conditions tested. Analysing the figure, it is possible to conclude that the axial force values for the three welds produced with the same traverse speed are close to each other, except in welds produced at 1000 mm/min. Considering all the welds performed, the torque and axial force seem not to have a relation. However, when analysed the welds produced with the same traverse speed and tool, it is possible to understand the relation. For the same traverse speed, when the axial force is higher, the torque is higher too.

### 4.3.2. Temperature Evolution with Process Parameters

Figure 4-19 Figure 4-20 show the thermal cycles registered at different rotational (800, 1000, 1600 rpm) and traverse speeds (600, 1000, 1400 mm/min), respectively. Analysing the figure it is possible to conclude that the shapes of the curves are very similar for the welds performed with the same traverse speed (Figure 4-19), but different for the welds performed with different traverse speeds (Figure 4-20). In fact, since the temperature evolution is plotted against the welding time, the curve is longer for the slower traverse speed. The shape of the curves also reflects the acceleration and deceleration periods, at the beginning and at the end of the welding, for the faster traverse speeds.

Analysing Figure 4-20, it can be concluded that the weld produced with the slow traverse speed reaches the highest temperature values. However, the temperature values are similar for the welds produced with 1000 mm/min and 1400 mm/min. To better compare the temperatures at the different weld speeds, the graph in Figure 4-21 was drawn.

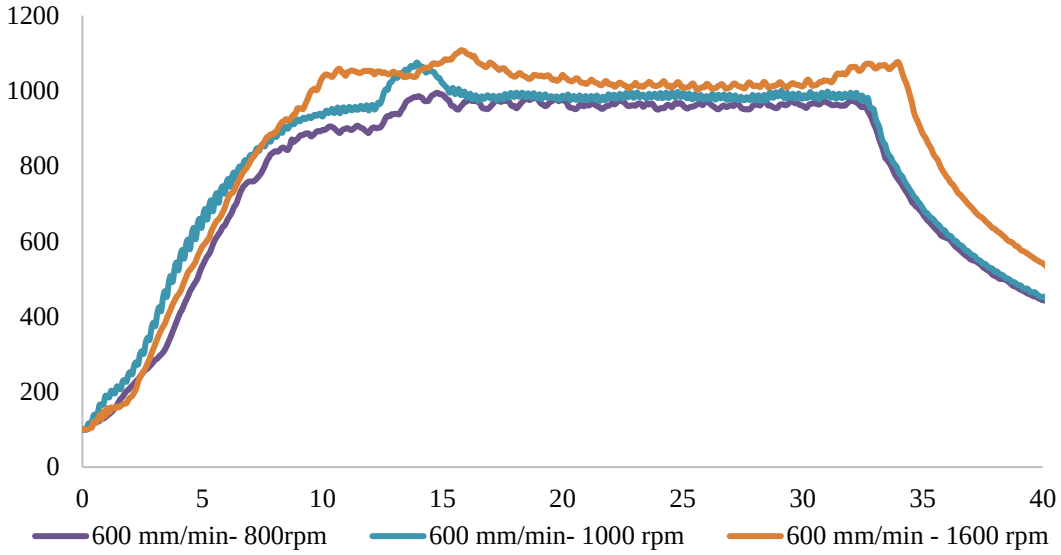


**Figure 4-19:** Temperature evolutions of the welds produced with PL16 tool at 600 mm/min.

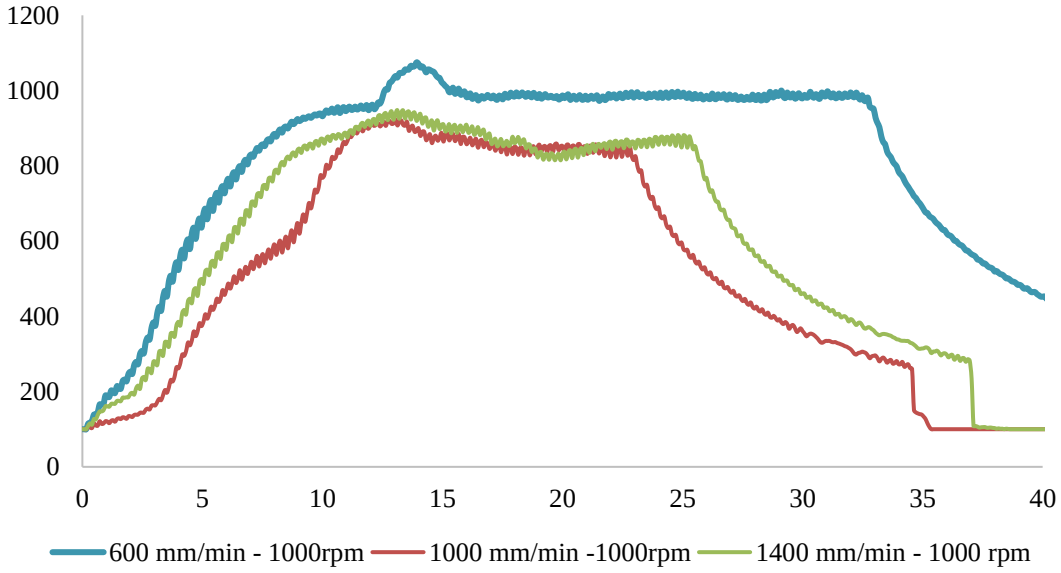


**Figure 4-20** Temperature evolutions of the welds produced with PL16 tool at 1000 rpm.

Analysing Figure 4-21, relative to the evolution of the average temperature with the speed ratio, it is possible to conclude that the traverse speed and the rotational speed have an influence on this output parameter. The welds produced at 600 mm/min traverse speed have higher values of average temperature when the rotational speed is higher. To the welds produced at 1000 and 1400 mm/min, when the rotational speed increases from 800 to 1000 rpm, the average temperature increases, but the opposite happens from 1000 to 1600 rpm. The average temperature values are higher for the welds produced with the slower traverse

speed (600 mm/min). The welds produced at 1000 and 1400 mm/min have a similar average temperature, except on the welds produced at 1600rpm, where the higher value is in the weld produced at 1000 mm/min.

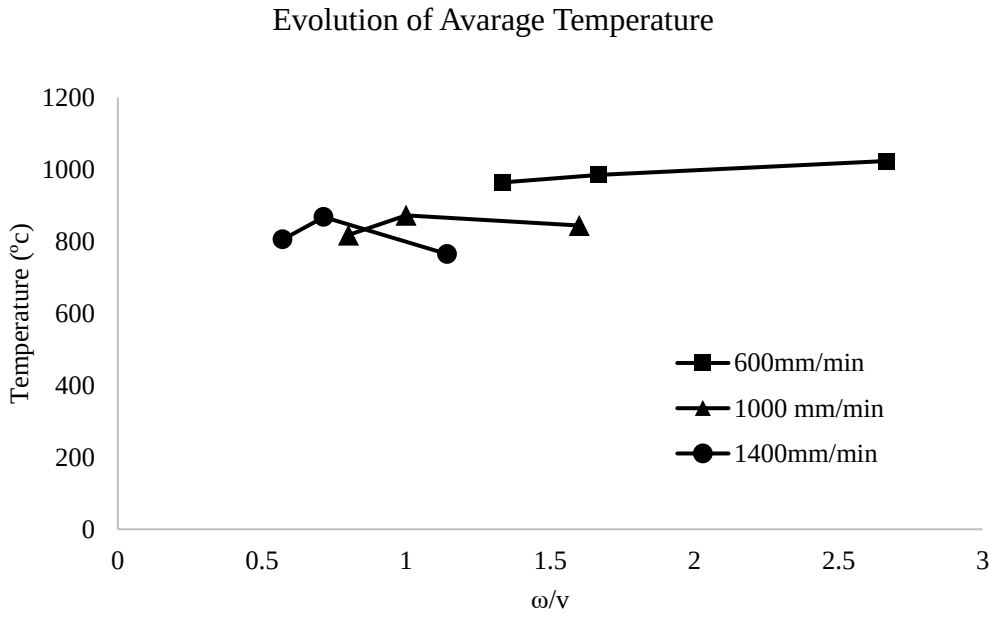


**Figure 4-21:** Evolution of Average Temperature with the speed ratio (ω/v).

The thermal cycle is a fundamental variable to understand the metallurgical transformations in the different PAZ of the welds. To better understand that influence, Figure 4-22 and Figure 4-23 show the average temperatures related to the weld's final width and PAZ height, respectively.

Figure 4-22 shows the evolution of the PAZ width with the temperature. The tendency line on this figure shows that the temperature has a relation with the width of the weld. Higher values of the temperature promote higher weld width. The figure also enables to conclude that a larger scatter in the PAZ width was registered for the welds performed at temperatures lower than 900 ºC and that the weld produced with the smaller width was the one produced at a lower temperature.

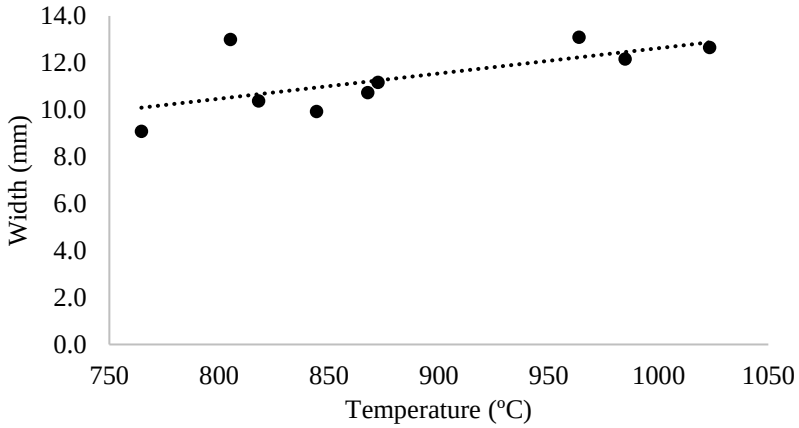


**Figure 4-22:** Evolution of Width with the Temperature.

Figure 4-23 shows the evolution of the height of the PAZ with the average welding temperature. The figure shows that the welds with the deeper PAZ were the ones produced at the higher welding temperature. As mentioned in the morphological and microstructural characterisation, the quality of the welds is related to the PAZ height, so it is possible to conclude that there is a relation between the quality of welds and the average temperature values. However, a poor quality weld was produced at a temperature of 860 ºC, higher than the temperature obtained to perform two good welds.

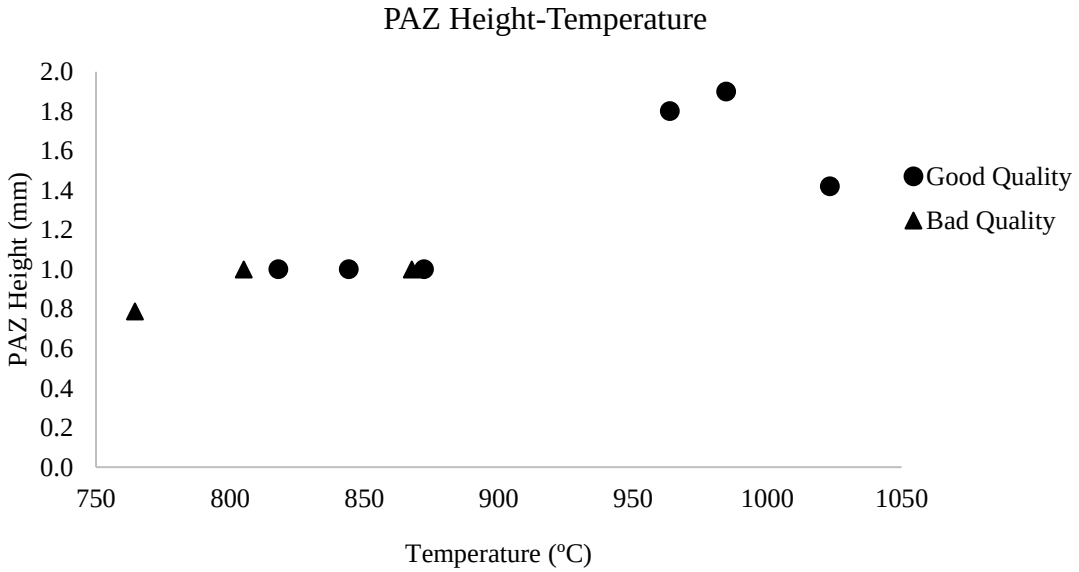


**Figure 4-23:** Height of Process Affected Zone to average temperature.

### 4.3.3. Separated Welds

As explained before, after the welds were produced, they were cut to create seven samples. Some of the samples were separated during the cut, showing that the weld was not of good quality. The welds for which that happened were produced with the PL12 tool, at 1000 and 1400 mm/min, and with the PL16 tool, at 1400 mm/min and 800 rpm and 1600 rpm. These welds will be analysed in this subchapter, with their output parameters.

These output parameters are plotted against distance. Figure 4-24Figure 4-25Figure 4-26Figure 4-27 show the evolution of the output parameters (Torque, Axial Force, Temperature), and of the traverse speed, with the tool displacement, as well as a photograph of the entire weld. The green rectangle in each figure identifies the weld portion for which effective bonding between the plates was registered, i.e., for which no separation between the plates occurred when handling the samples. On the other hand, the red rectangles represent the portion of the welds for which no effective bonding between the plates was registered.

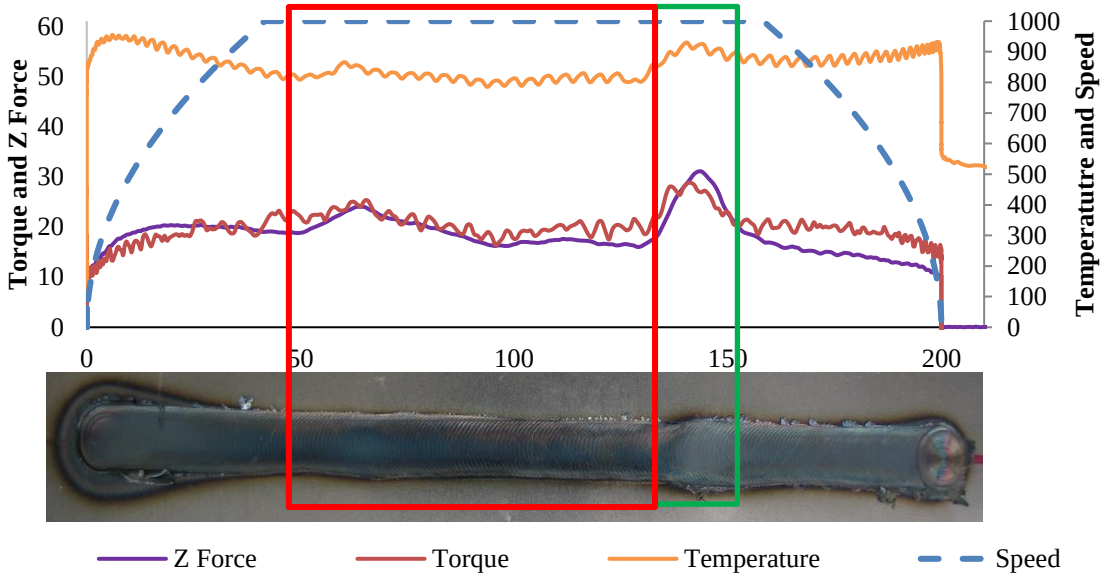


**Figure 4-24:** Weld produced with a PL12 tool at 1000 mm/min and 1000 rpm.

Analysing Figure 4-24, some conclusions can be drawn. Firstly, the relation between the torque and the axial force. In the same position, when the torque curve increases, there is also an increase of the axial force. Torque results were very sensitive to varying axial load. That can be observed in the 60 mm and 140 mm of the weld. Secondly, the weld width

is related to the temperature values, which can be observed in the weld between 140 mm and 200 mm. The value of the temperature is higher and the weld is larger on this localisation.

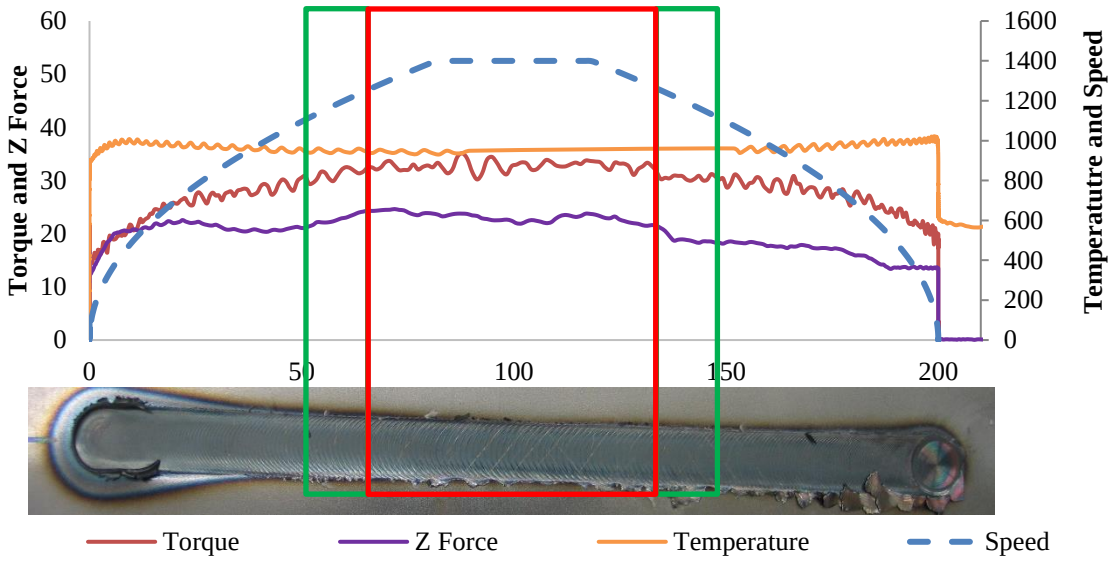


**Figure 4-25:** Weld produced with a PL12 tool at 1400 mm/min and 1000 rpm.

Although the weld in Figure 4-25 has a good appearance, the morphological analysis revealed that the PAZ ended at the final of the thickness of the upper plate, which can be observed in Figure 4-1. The weld was separated, but it was possible to obtain two samples, one for the metallurgical analysis and another for one tensile-shear test. The result of the tensile-shear test was not good, the sample broke in the weld zone at 1200 N. The evolution graphs of torque and axial force show a similar shape, during this welding, no significant peaks occurred. The temperature is practically constant throughout the weld, and so is the width of the weld.

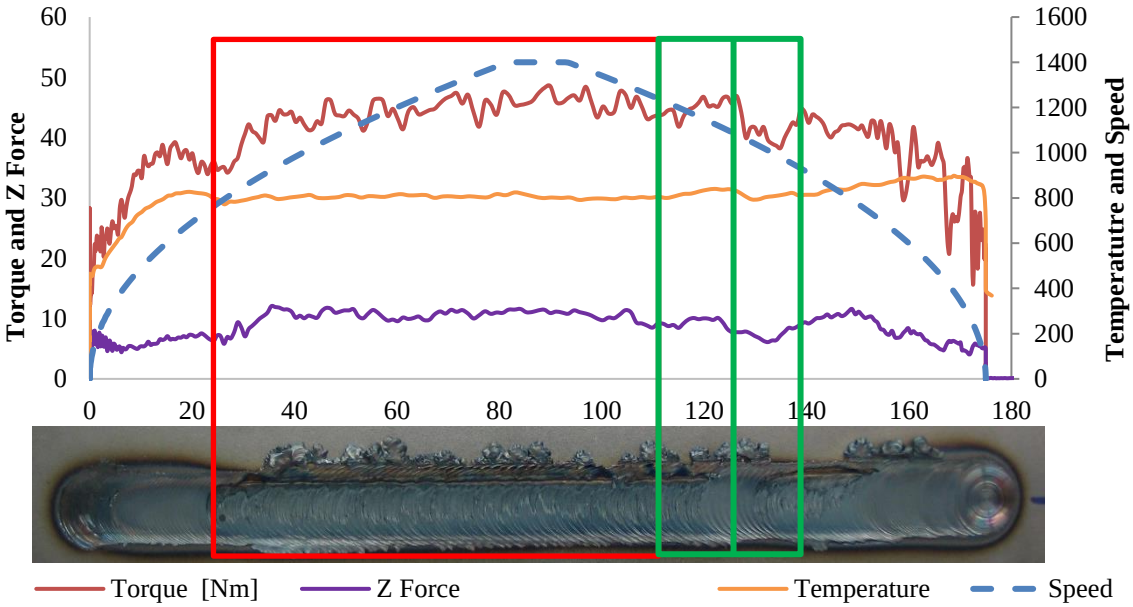


**Figure 4-26:** Weld produced with a PL16 tool at 1400 mm/min and 800 rpm.

The weld produced with a PL16 tool at 1400 mm/min and 800 rpm (Figure 4-26) has the worst appearance with flash defects and a lack of material practically all over the weld. However, two samples are obtained. The tensile-shear test made for one of the samples surprisingly got a good result. The base material broke away from the weld region at 3644N. Torque and axial force evolution suffer several oscillations, while the temperature and width are practically constant throughout the weld.

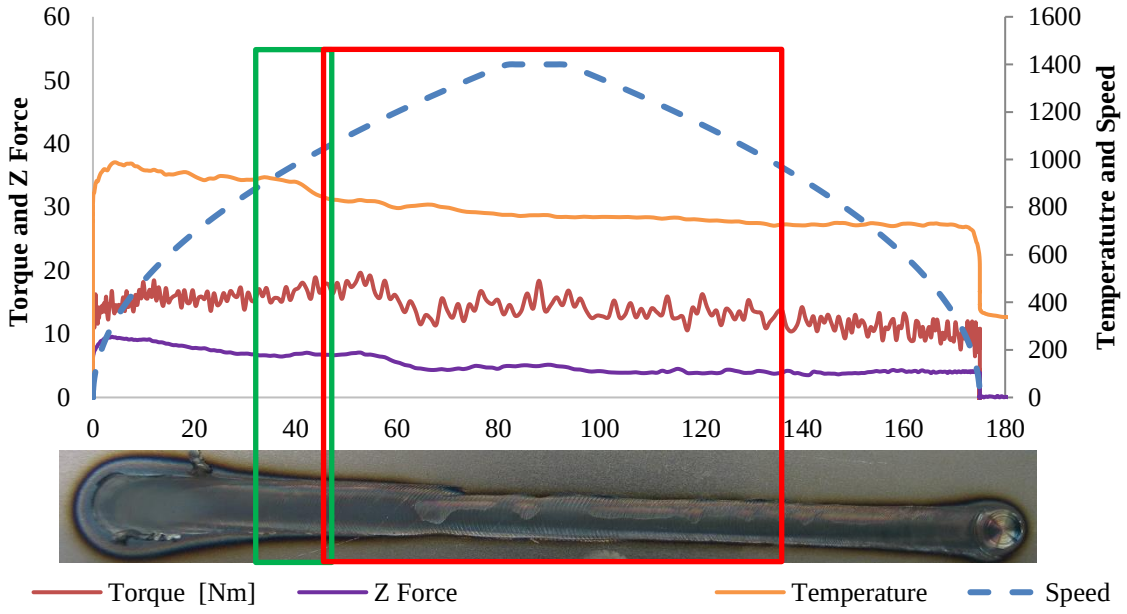


**Figure 4-27:** Weld produced with a PL16 tool at 1400 mm/min and 1600 rpm.

Lastly, analysing Figure 4-27, it is possible to conclude that the torque and the axial force have a relation, when one of them decreases, the other decreases. The temperature has a linear influence on the width of the weld. At the beginning of the welding, the temperature is maximum, and there is the maximum width, but the temperature starts to decrease, and the torque remains at the same value, the width of the weld starts decreasing too. In the 80 mm, the torque, temperature, axial force, and the weld width start to decrease until the end of the weld.

After analysing all the figures, it can be concluded that the Torque is sensitive to varying the axial force and the width of the weld is related to temperature because, in the locations where exists a temperature peak in the same location, the weld has a larger width. Another conclusion took for the welds produced at a traverse speed of 1400 mm/min is that all the samples cut in the region where the traverse speed is higher than 1200 mm/min are not joined.

# 5. CONCLUSIONS

The main objective of this work was to analyse the quality of welds in DC01 mild steel, produced using the Tool Assisted Friction Welding process, with different process parameters (traverse and rotational speeds and tool diameter). The welding torque and temperature were also related to the different input parameters and the quality of the welds. From this work, the following conclusions could be drawn:

- It is possible to produce steel lap welds with ultimate strength similar to the base material using TAFW. For all the welds produced in this work, the thickness reduction in the weld zone is practically nil compared with the base material thickness.
- The morphology of the welds evolves with the traverse and rotational speeds and the tool diameter. No hooking or cold lap defects were observed for practically all the welds, except the welds performed with the PL16 tool at 1400 mm/min and 800 and 1000 rpm.
- The traverse and rotational speed have a strong influence on the welding temperature.
- The rotational speed and the tool diameter influence the torque, but the traverse speed does not influence it.
- The axial force and the torque are related. When one increases instantly, the other also increases.
- The width of the weld surface is directly related to the temperature. When the temperature peak occurs, at that exact position, the weld width also is larger.
- The mechanical performance of the welds produced using 1400 mm/min is not good, have defects or unbonded interface.

Further analysis can still be done: Using different tool geometries; Produce the welds with a PL16 on traverse speed around 1200 mm/min to understand the real critical speed; Develop some intelligent data treatment software, Focus on the heat dissipation of the process.

# [BIBLIOGRAPHY]

Andrade, D. G., Leitão, C., Dialami, N., Chiumenti, M., & Rodrigues, D. M. (2020). Modelling torque and temperature in friction stir welding of aluminium alloys. *International Journal of Mechanical Sciences*, *182*(March). https://doi.org/10.1016/j.ijmecsci.2020.105725

Andrade, D. G., Leitão, C., & Rodrigues, D. M. (2018). Properties of lap welds in low carbon galvanised steel produced by tool assisted friction welding. *Journal of Materials Processing Technology*, *260*(December), 77–86. https://doi.org/10.1016/j.jmatprotec.2018.05.018

Andrade, D. G., Leitão, C., & Rodrigues, D. M. (2019). Influence of base material characteristics and process parameters on frictional heat generation during Friction Stir Spot Welding of steels. *Journal of Manufacturing Processes*, *43*(April), 98–104. https://doi.org/10.1016/j.jmapro.2019.05.015

Andrade, D. G., Sabari, S. S., Leitão, C., & Rodrigues, D. M. (2021). Influence of the galvanised coating thickness and process parameters on heat generation and strength of steel spot welds. *Thin-Walled Structures*, *160*(September 2020). https://doi.org/10.1016/j.tws.2020.107401

Bachmann, A., Gamper, J., Krutzlinger, M., Zens, A., & Zaeh, M. F. (2017). Adaptive model-based temperature control in friction stir welding. *International Journal of Advanced Manufacturing Technology*, *93*(1–4), 1157–1171. https://doi.org/10.1007/s00170-017-0594-5

Bakavos, D., Chen, Y., Babout, L., & Prangnell, P. (2011). Material interactions in a novel pinless tool approach to friction stir spot welding thin aluminum sheet. *Metallurgical and Materials Transactions A: Physical Metallurgy and Materials Science*, *42*(5), 1266–1282. https://doi.org/10.1007/s11661-010-0514-x

Bhushan, R. K., & Sharma, D. (2019). Green welding for various similar and dissimilar metals and alloys: present status and future possibilities. *Advanced Composites and Hybrid Materials*, *2*(3), 389–406. https://doi.org/10.1007/s42114-019-00094-8

Costa, M. I., Verdera, D., Leitão, C., & Rodrigues, D. M. (2015). Dissimilar friction stir lap welding of AA 5754-H22/AA 6082-T6 aluminium alloys: Influence of material properties and tool geometry on weld strength. *Materials and Design*, *87*, 721–731. https://doi.org/10.1016/j.matdes.2015.08.066

El-Sayed, M. M., Shash, A. Y., Abd-Rabou, M., & ElSherbiny, M. G. (2021). Welding and processing of metallic materials by using friction stir technique: A review. *Journal of Advanced Joining Processes*, *3*(January), 100059. https://doi.org/10.1016/j.jajp.2021.100059

Elangovan, K., Balasubramanian, V., & Valliappan, M. (2008). Influences of tool pin profile and axial force on the formation of friction stir processing zone in AA6061 aluminium alloy. *International Journal of Advanced Manufacturing Technology*, *38*(3–4), 285–295. https://doi.org/10.1007/s00170-007-1100-2

Forcellese, A., Gabrielli, F., & Simoncini, M. (2012). Mechanical properties and microstructure of joints in AZ31 thin sheets obtained by friction stir welding using "pin" and "pinless" tool configurations. *Materials and Design*, *34*, 219–229. https://doi.org/10.1016/j.matdes.2011.08.001

Galvão, I., Leitão, C., Loureiro, A., & Rodrigues, D. M. (2012). *Study of the welding conditions during similar and dissimilar aluminium and copper welding based on torque sensitivity analysis*. *42*, 259–264. https://doi.org/10.1016/j.matdes.2012.05.058

Kim, K. H., Bang, H. S., Bang, H. S., & Kaplan, A. F. H. (2017). Joint properties of ultra thin 430M2 ferritic stainless steel sheets by friction stir welding using pinless tool. *Journal of Materials Processing Technology*, *243*, 381–386. https://doi.org/10.1016/j.jmatprotec.2016.12.018

Lakshminarayanan, A. K., Annamalai, V. E., & Elangovan, K. (2015). Identification of optimum friction stir spot welding process parameters controlling the properties of low carbon automotive steel joints. *Journal of Materials Research and Technology*, *4*(3), 262–272. https://doi.org/10.1016/j.jmrt.2015.01.001

Leitão, C., Galvão, I., Leal, R. M., & Rodrigues, D. M. (2012). Determination of local constitutive properties of aluminium friction stir welds using digital image correlation. *Materials and Design*, *33*(1), 69–74. https://doi.org/10.1016/j.matdes.2011.07.009

Leitão, C., Louro, R., & Rodrigues, D. M. (2012). Using torque sensitivity analysis in

accessing Friction Stir Welding/Processing conditions. *Journal of Materials Processing Technology*, *212*(10), 2051–2057. https://doi.org/10.1016/j.jmatprotec.2012.05.009

Longhurst, W. R., Strauss, A. M., Cook, G. E., & Fleming, P. A. (2010). Torque control of friction stir welding for manufacturing and automation. *International Journal of Advanced Manufacturing Technology*, *51*(9–12), 905–913. https://doi.org/10.1007/s00170-010-2678-3

Mira-Aguiar, T., Verdera, D., Leitão, C., & Rodrigues, D. M. (2016). Tool assisted friction welding: A FSW related technique for the linear lap welding of very thin steel plates. *Journal of Materials Processing Technology*, *238*, 73–80. https://doi.org/10.1016/j.jmatprotec.2016.07.006

Mishra, R. S., & Ma, Z. Y. (2005). Friction stir welding and processing. *Materials Science and Engineering R: Reports*, *50*(1–2), 1–78. https://doi.org/10.1016/j.mser.2005.07.001

Nguyen, N. T., Kim, D. Y., & Kim, H. Y. (2011). Assessment of the failure load for an AA6061-T6 friction stir spot welding joint. *Proceedings of the Institution of Mechanical Engineers, Part B: Journal of Engineering Manufacture*, *225*(10), 1746–1756. https://doi.org/10.1177/0954405411405911

Ni, Y., Qin, D. Q., Mao, Y., Xiao, X., & Fu, L. (2020). Influences of welding parameters on axial force and deformations of micro pinless friction stir welding. *International Journal of Advanced Manufacturing Technology*, *106*(7–8), 3273–3283. https://doi.org/10.1007/s00170-019-04739-2

Oakes, T., & Landers, R. G. (2009). Design and implementation of a general tracking controller for friction stir welding processes. *Proceedings of the American Control Conference*, *2*, 5576–5581. https://doi.org/10.1109/ACC.2009.5160405

Rai, R., De, A., Bhadeshia, H. K. D. H., & DebRoy, T. (2011). Review: Friction stir welding tools. *Science and Technology of Welding and Joining*, *16*(4), 325–342. https://doi.org/10.1179/1362171811Y.0000000023

Silva-Magalhães, A., Cederqvist, L., De Backer, J., Håkansson, E., Ossiansson, B., & Bolmsjö, G. (2019). A Friction Stir Welding case study using Temperature Controlled Robotics with a HPDC Cylinder Block and dissimilar materials joining. *Journal of Manufacturing Processes*, *46*(August), 177–184.

https://doi.org/10.1016/j.jmapro.2019.08.012

Thomas, W. M., Johnson, K. I., & Wiesner, C. S. (2003). Friction stir welding-recent developments in tool and process technologies. *Advanced Engineering Materials*, *5*(7), 485–490. https://doi.org/10.1002/adem.200300355

Vural, M. (2014). Welding Processes and Technologies. In *Comprehensive Materials Processing* (Vol. 6). Elsevier. https://doi.org/10.1016/B978-0-08-096532-1.00603-8